

Batch Reinforcement Learning with a Nonparametric Off-Policy Policy Gradient

Samuele Tosatto, João Carvalho and Jan Peters

Abstract—Off-policy Reinforcement Learning (RL) holds the promise of better data efficiency as it allows sample reuse and potentially enables safe interaction with the environment. Current off-policy policy gradient methods either suffer from high bias or high variance, delivering often unreliable estimates. The price of inefficiency becomes evident in real-world scenarios such as interaction-driven robot learning, where the success of RL has been rather limited, and a very high sample cost hinders straightforward application. In this paper, we propose a nonparametric Bellman equation, which can be solved in closed form. The solution is differentiable w.r.t the policy parameters and gives access to an estimation of the policy gradient. In this way, we avoid the high variance of importance sampling approaches, and the high bias of semi-gradient methods. We empirically analyze the quality of our gradient estimate against state-of-the-art methods, and show that it outperforms the baselines in terms of sample efficiency on classical control tasks.

Index Terms—Reinforcement Learning, Policy Gradient, Nonparametric Estimation.

1 INTRODUCTION

REINFORCEMENT LEARNING has made overwhelming progress in recent years, especially when applied to board and computer games, or simulated tasks [1]–[3]. However, in comparison, only a little improvement has been achieved on real-world tasks. One of the reasons of this gap is that the vast majority of reinforcement learning approaches are on-policy. On-policy algorithms require that the samples are collected using the optimization policy; and therefore this implies that a) there is little control on the environment and b) samples must be discarded after each policy improvement, causing high sample inefficiency. In contrast, off-policy techniques are theoretically more sample efficient, because they decouple the procedures of data acquisition and policy update, allowing for the possibility of sample-reuse. Furthermore, off-policy estimation enables offline (or batch) reinforcement learning, which means that the algorithm extracts the optimal policy from a fixed dataset. This property is crucial in many real-world applications, since it allows a decoupled data-acquisition process, and, subsequently, a safer interaction with the environment. However, classical off-policy algorithms like Q-learning with function approximation and its offline version, fitted Q-iteration [4], [5], are not guaranteed to converge [6], [7], and allow only discrete actions. More recent semi-gradient¹ off-policy techniques, like Off-Policy Actor Critic (Off-PAC) [9], Deep Deterministic Policy Gradient (DDPG) [10], [11], Soft Actor Critic (SAC) [2], often perform sub-optimally, especially when the collected data is strongly off-policy, due to the biased semi-gradient update [12]. In the last years, offline techniques like Conservative Q-Learning (CQL) [13], Bootstrapping Error Accumulation

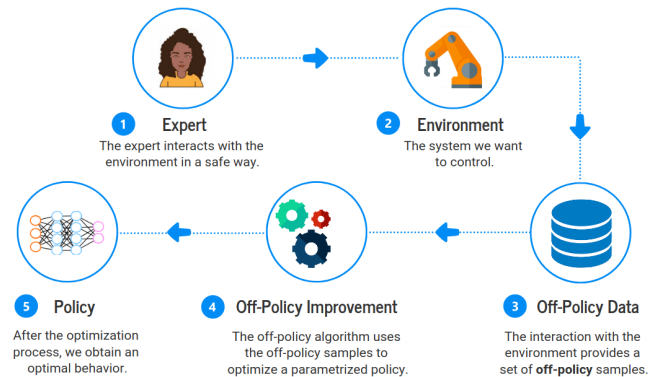


Fig. 1: In the off-policy reinforcement learning scheme, the policy can be optimized using an off-policy dataset. This allows for safer interaction with the system and for better sample efficiency.

Reduction (BEAR) [14] and Behavior Regularized Actor Critic (BRAC) [15], take care of a particular treatment of the out-of-distribution (OOD) policy improvement, however, still using the semi-gradient estimation. Another class of off-policy gradient estimation uses importance sampling [16]–[18] to deliver an unbiased estimate of the gradient but suffer from high variance and is generally only applicable with stochastic policies. Moreover, these algorithms require the full knowledge of the behavioral policy, making them unsuitable when data stems from a human demonstrator. On the other hand, model-based approaches aim to approximate the environment’s dynamics, allowing the generation of synthetic samples. The generative model can, in principle, be used by an on-policy reinforcement learning algorithm, therefore, encompassing the difficulty of off-policy estimation. However, the generation of synthetic samples is also problematic, as they are affected by the error of the approximated dynamics. To mitigate this problem, state-of-the-art techniques aim to quantify and penalize the

- Samuele Tosatto is with the University of Alberta, Edmonton, Alberta, Canada. Department of Computing Science. E-mail: tosatto@ualberta.ca.
- João Carvalho and Jan Peters are with the Technische Universität Darmstadt, Darmstadt, Germany, FG Intelligent Autonomous Systems. E-mail: {name}.{surname}@tu-darmstadt.de

1. We adopt the terminology from [8].

most uncertain regions of the state-action space, like Model-based Offline Policy Optimization (MOPO) [19] and Model-based Offline Reinforcement Learning (MOREL) [20]. To address all previously highlighted issues, we propose a new algorithm, the Nonparametric Off-policy Policy Gradient (NOPG) [21]. NOPG constructs a nonparametric model of the dynamics and the reward signal, and builds a full-gradient estimate based on the closed-form solution of a nonparametric Bellman equation. Our approach, in contrast to the majority of model-based approaches, does not require the generation of artificial data. On the other hand, while model-free approaches are either built on semi-gradient estimation, or importance sampling, NOPG computes a full-gradient estimate without importance sampling estimators, and allows for the use of human demonstrations. Figure 1 shows the offline scheme of NOPG. A behavioral policy, represented by a human demonstrator, provides (possibly suboptimal) trajectories that solve a task. NOPG optimizes a policy from off-line and off-policy samples.

Contribution. This paper introduces a nonparametric Bellman equation, and the full-gradient derived from its closed-form solution. We study the properties of the nonparametric Bellman equation, focusing on the bias of its closed-form solution. We empirically analyze the bias and the variance of the proposed gradient estimator. We compare its effectiveness and efficiency w.r.t. state of the art online and offline techniques, observing that NOPG exhibits high sample efficiency.

2 PROBLEM STATEMENT

Consider the reinforcement learning problem of an agent interacting with a given environment, as abstracted by a Markov decision process (MDP) and defined over the tuple $(\mathcal{S}, \mathcal{A}, \gamma, P, R, \mu_0)$ where $\mathcal{S} \equiv \mathbb{R}^{d_s}$ is the state space, $\mathcal{A} \equiv \mathbb{R}^{d_a}$ the action space, the transition-based discount factor γ is a stochastic mapping between $\mathcal{S} \times \mathcal{A} \times \mathcal{S}$ to $[0, 1)$, which allows for unification of episodic and continuing tasks [22]. The discount factor allows the transformation of a particular MDP to an equivalent MDP where, at each state-action, there is $1 - \gamma$ probability to transition to an absorbing state with zero reward. A variable discount factor, can, therefore, be interpreted as a variable probability of transitioning to an absorbing state. To keep however the theory simple, we will assume that $\gamma(\mathbf{s}, \mathbf{a}, \mathbf{s}') \leq \gamma_c$ where $\gamma_c < 1$. The transition probability from a state \mathbf{s} to \mathbf{s}' given an action \mathbf{a} is governed by the conditional density $p(\mathbf{s}'|\mathbf{s}, \mathbf{a})$. The stochastic reward signal R for a transition $(\mathbf{s}, \mathbf{a}, \mathbf{s}') \in \mathcal{S} \times \mathcal{A} \times \mathcal{S}$ is drawn from a distribution $R(\mathbf{s}, \mathbf{a}, \mathbf{s}')$ with mean value $\mathbb{E}_{\mathbf{s}'}[R(\mathbf{s}, \mathbf{a}, \mathbf{s}')] = r(\mathbf{s}, \mathbf{a})$. The initial distribution $\mu_0(\mathbf{s})$ denotes the probability of the state $\mathbf{s} \in \mathcal{S}$ to be a starting state. A policy π is a stochastic or deterministic mapping from \mathcal{S} onto \mathcal{A} , usually parametrized by a set of parameters θ .

We define an *episode* as $\tau \equiv \{\mathbf{s}_t, \mathbf{a}_t, r_t, \gamma_t\}_{t=1}^{\infty}$ where

$$\begin{aligned} \mathbf{s}_0 &\sim \mu_0(\cdot); & \mathbf{a}_t &\sim \pi(\cdot | \mathbf{s}_t); & \mathbf{s}_{t+1} &\sim p(\cdot | \mathbf{s}_t, \mathbf{a}_t) \\ r_t &\sim R(\mathbf{s}_t, \mathbf{a}_t, \mathbf{s}_{t+1}); & \gamma_t &\sim \gamma(\mathbf{s}_t, \mathbf{a}_t, \mathbf{s}_{t+1}). \end{aligned}$$

In this paper we consider the discounted infinite-horizon setting, where the objective is to maximize the expected return

$$J_\pi = \mathbb{E}_\tau \left[\sum_{t=0}^{\infty} r_t \prod_{i=0}^t \gamma_i \right]. \quad (1)$$

It is important to introduce two important quantities: the *stationary state visitation* μ_π and the *value function* V_π . We naturally extend the stationary state visitation defined by [23] with the transition-based discount factor

$$\mu(\mathbf{s}) = \mathbb{E}_\tau \left[\sum_{t=0}^{\infty} p(\mathbf{s} = \mathbf{s}_t | \pi, \mu_0) \prod_{i=1}^t \gamma_i \right],$$

or, equivalently, as the fixed point of

$$\mu(\mathbf{s}) = \mu_0(\mathbf{s}) + \int_{\mathcal{S}} \int_{\mathcal{A}} p_\gamma(\mathbf{s}|\mathbf{s}', \mathbf{a}') \pi(\mathbf{a}'|\mathbf{s}') \mu_\pi(\mathbf{s}') d\mathbf{s}' d\mathbf{a}'$$

where, from now on, $p_\gamma(\mathbf{s}'|\mathbf{s}, \mathbf{a}) = p(\mathbf{s}'|\mathbf{s}, \mathbf{a})\mathbb{E}[\gamma(\mathbf{s}, \mathbf{a}, \mathbf{s}')]$. The value function

$$V_\pi(\mathbf{s}) = \mathbb{E}_\tau \left[\sum_{t=0}^{\infty} r_t p(r_t | \mathbf{s}_0 = \mathbf{s}, \pi) \prod_{i=0}^t \gamma_i \right],$$

corresponds to the fixed point of the Bellman equation,

$$V_\pi(\mathbf{s}) = \int_{\mathcal{A}} \pi(\mathbf{a}|\mathbf{s}) \left(r(\mathbf{s}, \mathbf{a}) + \int_{\mathcal{S}} V_\pi(\mathbf{s}') p_\gamma(\mathbf{s}'|\mathbf{s}, \mathbf{a}) d\mathbf{s}' \right) d\mathbf{a}.$$

The state-action value function is defined as

$$Q_\pi(\mathbf{s}, \mathbf{a}) = r(\mathbf{s}, \mathbf{a}) + \int_{\mathcal{S}} V_\pi(\mathbf{s}') p_\gamma(\mathbf{s}'|\mathbf{s}, \mathbf{a}) d\mathbf{s}'.$$

The expected return (1) can be formulated as

$$J_\pi = \int_{\mathcal{S}} \mu_0(\mathbf{s}) V_\pi(\mathbf{s}) d\mathbf{s} = \int_{\mathcal{S}} \int_{\mathcal{A}} \mu_\pi(\mathbf{s}) \pi(\mathbf{a}|\mathbf{s}) r(\mathbf{s}, \mathbf{a}) d\mathbf{a} d\mathbf{s}.$$

Policy Gradient Theorem. Objective (1) is usually maximized via gradient ascent. The gradient of J_π w.r.t. the policy parameters θ is

$$\nabla_\theta J_\pi = \int_{\mathcal{S}} \int_{\mathcal{A}} \mu_\pi(\mathbf{s}) \pi_\theta(\mathbf{a}|\mathbf{s}) Q_\pi(\mathbf{s}, \mathbf{a}) \nabla_\theta \log \pi_\theta(\mathbf{a}|\mathbf{s}) d\mathbf{a} d\mathbf{s},$$

as stated in the policy gradient theorem [23]. When it is possible to interact with the environment with the policy π_θ , one can approximate the integral by considering the state-action as a distribution (up to a normalization factor) and use the samples to perform a Monte-Carlo (MC) estimation [24]. The Q -function can be estimated via Monte-Carlo sampling, approximate dynamic programming or by direct Bellman minimization. In the off-policy setting, we do not have access to the state-visitation μ_π induced by the policy, but instead we observe a different state distribution. While estimating the Q -function with the new state distribution is well established in the literature [4], [25], the shift in the state visitation $\mu_\pi(\mathbf{s})$ is more difficult to obtain. State-of-the-art techniques either omit to consider this shift (we refer to these algorithms as *semi-gradient*), or they try to estimate it via importance sampling correction. These approaches will be discussed in detail in Section 4.

3 NONPARAMETRIC OFF-POLICY POLICY GRADIENT

In this section, we introduce a nonparametric Bellman equation with a closed form solution, which carries the dependency from the policy's parameters. We derive the gradient of the solution, and discuss the properties of the proposed estimator.

3.1 A Nonparametric Bellman Equation

Nonparametric methods, require the storage of all samples to make predictions, but usually exhibit a low bias. They gained popularity thanks to their general simplicity and their theoretical properties. In this paper, we focus on kernel density estimation, and Nadaraya-Watson kernel regression. In this context, it is usual to assume the kernel to be a symmetric, real function κ , with positive co-domain and with $\int k(x, y) dx = 1 \forall y$. The goal of kernel density estimation is to predict the density of a distribution $p(\mathbf{s})$. After the collection of n samples $\mathbf{x}_i \sim p(\cdot)$, it is possible to obtain the estimated density

$$\hat{p}(\mathbf{x}) = n^{-1} \sum_{i=1}^n \kappa(\mathbf{x}, \mathbf{x}_i).$$

Nadaraya-Watson kernel regression builds on the kernel density estimation to predict the output of a function $f : \mathbb{R}^d \rightarrow \mathbb{R}$, assuming to observe a dataset of n samples $\{\mathbf{x}_i, y_i\}_{i=1}^n$ with $\mathbf{x}_i \sim p(\cdot)$ and $y_i = f(\mathbf{x}_i) + \epsilon_i$ (where ϵ_i is a zero-mean noise with finite variance). The prediction

$$\hat{f}(\mathbf{x}) = \frac{\int_{\mathbb{R}} y \hat{p}(\mathbf{x}, y) dy}{\hat{p}(\mathbf{x})} = \frac{\sum_{i=1}^n y_i \kappa(\mathbf{x}, \mathbf{x}_i)}{\sum_{i=1}^n \kappa(\mathbf{x}, \mathbf{x}_i)}$$

is constructed on the expectation of the conditional density probability, keeping in account that $\int_{\mathbb{R}} y \kappa(y, y_i) dy = y_i$. Nonparametric Bellman equations have been developed in a number of prior works. [26]–[28] used nonparametric models such as Gaussian Processes for approximate dynamic programming. [29] have shown that these methods differ mainly in their use of regularization. [30] provided a Bellman equation using kernel density-estimation and a general overview on nonparametric dynamic programming. In contrast to prior work, our formulation preserves the dependency on the policy, enabling the computation of the policy gradient in closed-form. Moreover, we upper-bound the bias of the Nadaraya-Watson kernel regression to prove that our value function estimate is consistent w.r.t. the classical Bellman equation under smoothness assumptions. We focus on the maximization of the average return in the infinite horizon case formulated as a starting state objective $\int_{\mathcal{S}} \mu_0(\mathbf{s}) V_{\pi}(\mathbf{s}) ds$ [23].

Definition 1. *The discounted infinite-horizon objective is defined by $J_{\pi} = \int \mu_0(\mathbf{s}) V_{\pi}(\mathbf{s}) ds$. Under a stochastic policy the objective is subject to the Bellman equation constraint*

$$V_{\pi}(\mathbf{s}) = \int_{\mathcal{A}} \pi_{\theta}(\mathbf{a}|\mathbf{s}) \left(r(\mathbf{s}, \mathbf{a}) + \gamma \int_{\mathcal{S}} V_{\pi}(\mathbf{s}') p(\mathbf{s}'|\mathbf{s}, \mathbf{a}) ds' \right) d\mathbf{a}, \quad (2)$$

while in the case of a deterministic policy the constraint is given as

$$V_{\pi}(\mathbf{s}) = r(\mathbf{s}, \pi_{\theta}(\mathbf{s})) + \gamma \int_{\mathcal{S}} V_{\pi}(\mathbf{s}') p(\mathbf{s}'|\mathbf{s}, \pi_{\theta}(\mathbf{s})) ds'.$$

Maximizing the objective in Definition 1 analytically is not possible, excluding special cases such as under linear-quadratic assumptions [31], or finite state-action space. Extracting an expression for the gradient of J_{π} w.r.t. the policy parameters θ is also not straightforward given the infinite set of possibly non-convex constraints represented in the recursion over V_{π} . Nevertheless, it is possible to transform the constraints in Definition 1 to a finite set of linear constraints via nonparametric modeling, thus leading to an expression of the value function with simple algebraic manipulation [30].

3.1.1 Nonparametric Modeling.

Assume a set of n observations $D \equiv \{\mathbf{s}_i, \mathbf{a}_i, r_i, \mathbf{s}'_i, \gamma_i\}_{i=1}^n$ sampled from interaction with an environment, with $\mathbf{s}_i, \mathbf{a}_i \sim \beta(\cdot, \cdot)$, $\mathbf{s}'_i \sim p(\cdot|\mathbf{s}_i, \mathbf{a}_i)$, $r_i \sim R(\mathbf{s}_i, \mathbf{a}_i)$ and $\gamma \sim \gamma(\mathbf{s}_i, \mathbf{a}_i, \mathbf{s}'_i)$. We define the kernels $\psi : \mathcal{S} \times \mathcal{S} \rightarrow \mathbb{R}^+$, $\varphi : \mathcal{A} \times \mathcal{A} \rightarrow \mathbb{R}^+$ and $\phi : \mathcal{S} \times \mathcal{S} \rightarrow \mathbb{R}^+$, as normalized, symmetric and positive definite functions with bandwidths $\mathbf{h}_{\psi}, \mathbf{h}_{\varphi}, \mathbf{h}_{\phi}$ respectively. We define $\psi_i(\mathbf{s}) = \psi(\mathbf{s}, \mathbf{s}_i)$, $\varphi_i(\mathbf{a}) = \varphi(\mathbf{a}, \mathbf{a}_i)$, and $\phi_i(\mathbf{s}) = \phi(\mathbf{s}, \mathbf{s}'_i)$. Following [30], the mean reward $r(\mathbf{s}, \mathbf{a})$ and the transition conditional $p(\mathbf{s}'|\mathbf{s}, \mathbf{a})$ are approximated by the Nadaraya-Watson regression [32], [33] and kernel density estimation, respectively

$$\begin{aligned} \hat{r}(\mathbf{s}, \mathbf{a}) &:= \frac{\sum_{i=1}^n \psi_i(\mathbf{s}) \varphi_i(\mathbf{a}) r_i}{\sum_{i=1}^n \psi_i(\mathbf{s}) \varphi_i(\mathbf{a})}, \\ \hat{p}(\mathbf{s}'|\mathbf{s}, \mathbf{a}) &:= \frac{\sum_{i=1}^n \phi_i(\mathbf{s}') \psi_i(\mathbf{s}) \varphi_i(\mathbf{a})}{\sum_{i=1}^n \psi_i(\mathbf{s}) \varphi_i(\mathbf{a})}, \\ \hat{\gamma}(\mathbf{s}, \mathbf{a}, \mathbf{s}') &:= \frac{\sum_{i=1}^n \gamma_i \psi_i(\mathbf{s}) \varphi_i(\mathbf{a}) \phi_i(\mathbf{s}')}{\sum_{i=1}^n \psi_i(\mathbf{s}) \varphi_i(\mathbf{a}) \phi_i(\mathbf{s}')} \end{aligned}$$

and, therefore, by the product of \hat{p} and $\hat{\gamma}$ we obtain

$$\begin{aligned} \hat{p}_{\gamma}(\mathbf{s}'|\mathbf{s}, \mathbf{a}) &:= \hat{p}(\mathbf{s}'|\mathbf{s}, \mathbf{a}) \hat{\gamma}(\mathbf{s}, \mathbf{a}, \mathbf{s}') \\ &= \frac{\sum_{i=1}^n \gamma_i \psi_i(\mathbf{s}) \varphi_i(\mathbf{a}) \phi_i(\mathbf{s}')}{\sum_{i=1}^n \psi_i(\mathbf{s}) \varphi_i(\mathbf{a})}. \end{aligned}$$

Inserting the reward and transition kernels into the Bellman Equation for the stochastic policy case we obtain the nonparametric Bellman equation (NPBE)

$$\begin{aligned} \hat{V}_{\pi}(\mathbf{s}) &= \int_{\mathcal{A}} \pi_{\theta}(\mathbf{a}|\mathbf{s}) \left(\hat{r}(\mathbf{s}, \mathbf{a}) + \int_{\mathcal{S}} \hat{V}_{\pi}(\mathbf{s}') \hat{p}_{\gamma}(\mathbf{s}'|\mathbf{s}, \mathbf{a}) ds' \right) d\mathbf{a} \\ &= \sum_i \int_{\mathcal{A}} \frac{\pi_{\theta}(\mathbf{a}|\mathbf{s}) \psi_i(\mathbf{s}) \varphi_i(\mathbf{a})}{\sum_j \psi_j(\mathbf{s}) \varphi_j(\mathbf{a})} d\mathbf{a} \\ &\quad \times \left(r_i + \gamma_i \int_{\mathcal{S}} \phi_i(\mathbf{s}') \hat{V}_{\pi}(\mathbf{s}') ds' \right). \quad (3) \end{aligned}$$

Equation (3) can be conveniently expressed in matrix form by introducing the vector of responsibilities $\varepsilon_i(\mathbf{s}) = \int \pi_{\theta}(\mathbf{a}|\mathbf{s}) \psi_i(\mathbf{s}) \varphi_i(\mathbf{a}) / \sum_j \psi_j(\mathbf{s}) \varphi_j(\mathbf{a}) d\mathbf{a}$, which assigns each state \mathbf{s} a weight relative to its distance to a sample i under the current policy.

Definition 2. *The nonparametric Bellman equation on the dataset D is formally defined as*

$$\hat{V}_{\pi}(\mathbf{s}) = \varepsilon_{\pi}^T(\mathbf{s}) \left(\mathbf{r} + \int_{\mathcal{S}} \phi_{\gamma}(\mathbf{s}') \hat{V}_{\pi}(\mathbf{s}') ds' \right), \quad (4)$$

with $\phi_\gamma(\mathbf{s}) = [\gamma_1 \phi_1(\mathbf{s}), \dots, \gamma_n \phi_n(\mathbf{s})]^\top$, $\mathbf{r} = [r_1, \dots, r_n]^\top$, $\boldsymbol{\varepsilon}_\pi(\mathbf{s}) = [\varepsilon_1^\pi(\mathbf{s}), \dots, \varepsilon_n^\pi(\mathbf{s})]^\top$,

$$\varepsilon_i(\mathbf{s}, \mathbf{a}) = \frac{\psi_i(\mathbf{s}) \varphi_i(\mathbf{a})}{\sum_j \psi_j(\mathbf{s}) \varphi_j(\mathbf{a})}$$

and

$$\varepsilon_i^\pi(\mathbf{s}) = \begin{cases} \int \pi_\theta(\mathbf{a}|\mathbf{s}) \varepsilon_i(\mathbf{s}, \mathbf{a}) \, \mathrm{d}\mathbf{a} & \text{if } \pi \text{ is stochastic} \\ \varepsilon_i(\mathbf{s}, \pi_\theta(\mathbf{s})) & \text{otherwise.} \end{cases}$$

From Equation (4) we deduce that the value function must be of the form $\boldsymbol{\varepsilon}_\pi^\top(\mathbf{s}) \mathbf{q}_\pi$, indicating that it can also be seen as a form of Nadaraya-Watson kernel regression,

$$\boldsymbol{\varepsilon}_\pi^\top(\mathbf{s}) \mathbf{q}_\pi = \boldsymbol{\varepsilon}_\pi^\top(\mathbf{s}) \left(\mathbf{r} + \int_{\mathcal{S}} \phi_\gamma(\mathbf{s}') \boldsymbol{\varepsilon}_\pi^\top(\mathbf{s}') \mathbf{q}_\pi \, \mathrm{d}\mathbf{s}' \right). \quad (5)$$

Notice that, trivially, every \mathbf{q}_π which satisfies

$$\mathbf{q}_\pi = \mathbf{r} + \int_{\mathcal{S}} \phi_\gamma(\mathbf{s}') \boldsymbol{\varepsilon}_\pi^\top(\mathbf{s}') \mathbf{q}_\pi \, \mathrm{d}\mathbf{s}' \quad (6)$$

also satisfies Equation (5). Theorem 1 demonstrates that the algebraic solution of Equation (6) is the *only* solution of the nonparametric Bellman Equation (4).

Theorem 1. *The nonparametric Bellman equation has a unique fixed-point solution*

$$\hat{V}_\pi^*(\mathbf{s}) := \boldsymbol{\varepsilon}_\pi^\top(\mathbf{s}) \boldsymbol{\Lambda}_\pi^{-1} \mathbf{r},$$

with $\boldsymbol{\Lambda}_\pi := I - \hat{\mathbf{P}}_\pi^\gamma$ and $\hat{\mathbf{P}}_\pi^\gamma := \int_{\mathcal{S}} \phi_\gamma(\mathbf{s}') \boldsymbol{\varepsilon}_\pi^\top(\mathbf{s}') \, \mathrm{d}\mathbf{s}'$, where $\boldsymbol{\Lambda}_\pi$ is always invertible since $\hat{\mathbf{P}}_\pi^{\pi, \gamma}$ is a strictly sub-stochastic matrix (Frobenius' Theorem). The statement is valid also for $n \rightarrow \infty$, provided bounded R .

The transition matrix $\hat{\mathbf{P}}_\pi^\gamma$ is strictly sub-stochastic since each row $\hat{\mathbf{P}}_{\pi, i}^\gamma = \gamma_i \int \phi_i(\mathbf{s}') \boldsymbol{\varepsilon}_\pi^\top(\mathbf{s}') \, \mathrm{d}\mathbf{s}'$ is composed by the convolution between ϕ_i , which by definition integrates to one, and $0 \leq \varepsilon_i^\pi(\mathbf{s}') \leq 1$, as can be seen in Definition 2. Proof of Theorem 1 is provided in the supplementary material.

3.2 Nonparametric Gradient Estimation

With the closed-form solution of $\hat{V}_\pi^*(\mathbf{s})$ from Theorem 1, it is possible to compute the analytical gradient of \hat{J}_π w.r.t. the policy parameters

$$\begin{aligned} \nabla_\theta \hat{V}_\pi^*(\mathbf{s}) &= \left(\frac{\partial}{\partial \theta} \boldsymbol{\varepsilon}_\pi^\top(\mathbf{s}) \right) \boldsymbol{\Lambda}_\pi^{-1} \mathbf{r} + \boldsymbol{\varepsilon}_\pi^\top(\mathbf{s}) \frac{\partial}{\partial \theta} \boldsymbol{\Lambda}_\pi^{-1} \mathbf{r} \\ &= \underbrace{\left(\frac{\partial}{\partial \theta} \boldsymbol{\varepsilon}_\pi^\top(\mathbf{s}) \right) \boldsymbol{\Lambda}_\pi^{-1} \mathbf{r}}_A \\ &\quad + \underbrace{\boldsymbol{\varepsilon}_\pi^\top(\mathbf{s}) \boldsymbol{\Lambda}_\pi^{-1} \left(\frac{\partial}{\partial \theta} \hat{\mathbf{P}}_\pi^\gamma \right) \boldsymbol{\Lambda}_\pi^{-1} \mathbf{r}}_B. \end{aligned} \quad (7)$$

Substituting the result of Equation (7) into the return specified in Definition 1, introducing $\boldsymbol{\varepsilon}_{\pi,0}^\top := \int \mu_0(\mathbf{s}) \boldsymbol{\varepsilon}_\pi^\top(\mathbf{s}) \, \mathrm{d}\mathbf{s}$, $\mathbf{q}_\pi = \boldsymbol{\Lambda}_\pi^{-1} \mathbf{r}$, and $\boldsymbol{\mu}_\pi = \boldsymbol{\Lambda}_\pi^{-\top} \boldsymbol{\varepsilon}_{\pi,0}$, we obtain

$$\nabla_\theta \hat{J}_\pi = \left(\frac{\partial}{\partial \theta} \boldsymbol{\varepsilon}_{\pi,0}^\top \right) \mathbf{q}_\pi + \boldsymbol{\mu}_\pi^\top \left(\frac{\partial}{\partial \theta} \hat{\mathbf{P}}_\pi^\gamma \right) \mathbf{q}_\pi, \quad (8)$$

Algorithm 1 Nonparametric Off-Policy Policy Gradient

input: dataset $\{\mathbf{s}_i, \mathbf{a}_i, r_i, \mathbf{s}'_i, \gamma_i\}_{i=1}^n$ where π_θ indicates the policy to optimize and ψ, ϕ, φ the kernels respectively for state, action and next-state.

while not converged **do**

 Compute $\boldsymbol{\varepsilon}_\pi^\top(\mathbf{s})$ as in Definition 2 and $\boldsymbol{\varepsilon}_{\pi,0}^\top := \int \mu_0(\mathbf{s}) \boldsymbol{\varepsilon}_\pi^\top(\mathbf{s}) \, \mathrm{d}\mathbf{s}$.

 Estimate $\hat{\mathbf{P}}_\pi^\gamma$ as defined in Theorem 1 using MC ($\phi(\mathbf{s})$ is a distribution).

 Solve $\mathbf{r} = \boldsymbol{\Lambda}_\pi \mathbf{q}_\pi$ and $\boldsymbol{\varepsilon}_{\pi,0} = \boldsymbol{\Lambda}_\pi^\top \boldsymbol{\mu}_\pi$ for \mathbf{q}_π and $\boldsymbol{\mu}_\pi$ using conjugate gradient.

 Update θ using Equation (8).

end while

where \mathbf{q}_π and $\boldsymbol{\mu}_\pi$ can be estimated via conjugate gradient to avoid the inversion of $\boldsymbol{\Lambda}_\pi$. It is interesting to notice that (8) is closely related to the Policy Gradient Theorem [23],

$$\nabla_\theta \hat{J}_\pi = \int_{\mathcal{S} \times \mathcal{A}} \underbrace{(\mu_0(\mathbf{s}) + \phi_\gamma^\top(\mathbf{s}) \boldsymbol{\mu}_\pi)}_{\text{Stationary distribution}} \underbrace{\boldsymbol{\varepsilon}^\top(\mathbf{s}, \mathbf{a}) \mathbf{q}_\pi}_{\hat{Q}_\pi(\mathbf{s}, \mathbf{a})} \nabla_\theta \pi_\theta(\mathbf{a}|\mathbf{s}) \, \mathrm{d}\mathbf{s} \, \mathrm{d}\mathbf{a}$$

and to the Deterministic Policy Gradient Theorem (in its onpolicy formulation) [10],

$$\nabla_\theta \hat{J}_\pi = \int_{\mathcal{S}} \underbrace{(\mu_0(\mathbf{s}) + \phi_\gamma^\top(\mathbf{s}) \boldsymbol{\mu}_\pi)}_{\text{Stationary distribution}} \underbrace{\nabla_{\mathbf{a}} \boldsymbol{\varepsilon}^\top(\mathbf{s}, \mathbf{a}) \mathbf{q}_\pi}_{\nabla_{\mathbf{a}} \hat{Q}_\pi(\mathbf{s}, \mathbf{a})} \nabla_\theta \pi_\theta(\mathbf{s}) \, \mathrm{d}\mathbf{s}.$$

In a later analysis, we will consider the state-action surrogate return $J_S^\pi(\mathbf{s}, \mathbf{a}) = (\mu_0(\mathbf{s}) + \phi_\gamma^\top(\mathbf{s}) \boldsymbol{\mu}_\pi) \boldsymbol{\varepsilon}^\top(\mathbf{s}, \mathbf{a}) \mathbf{q}_\pi$. The terms A and B in Equation (7) correspond to the terms in Equation (10). In contrast to semi-gradient actor-critic methods, where the gradient bias is affected by both the critic bias and the semi-gradient approximation [8], [12], our estimate is the *full gradient* and the only source of bias is introduced by the estimation of \hat{V}_π , which we analyze in Section 3.3. The term $\boldsymbol{\mu}_\pi$ can be interpreted as the support of the state-distribution as it satisfies $\boldsymbol{\mu}_\pi^\top = \boldsymbol{\varepsilon}_{\pi,0}^\top + \boldsymbol{\mu}_\pi^\top \hat{\mathbf{P}}_\pi^\gamma$. In Section 5, more specifically in Figure 7, we empirically show that $\boldsymbol{\varepsilon}_\pi^\top(\mathbf{s}) \boldsymbol{\mu}_\pi$ provides an estimate of the state distribution over the whole state-space. The quantities $\boldsymbol{\varepsilon}_{\pi,0}^\top$ and $\hat{\mathbf{P}}_{i,j}^\pi$ are estimated via Monte-Carlo sampling, which is unbiased but computationally demanding, or using other techniques such as unscented transform or numerical quadrature. The matrix $\hat{\mathbf{P}}_\pi^\gamma$ is of dimension $n \times n$, which can be memory-demanding. In practice, we notice that the matrix is often sparse. By taking advantage of conjugate gradient and sparsification we are able to achieve computational complexity of $\mathcal{O}(n^2)$ per policy update and memory complexity of $\mathcal{O}(n)$. Further details on the computational and memory complexity can be found in the supplementary material. A schematic of our implementation is summarized in Algorithm 1.

3.3 A theoretical Analysis

Nonparametric estimates of the transition dynamics and reward enjoy favorable properties for an off-policy learn-

ing setting. A well-known asymptotic behavior of the Nadaraya-Watson kernel regression,

$$\mathbb{E} \left[\lim_{n \rightarrow \infty} \hat{f}_n(x) \right] - f(x) \approx h_n^2 \left(\frac{1}{2} f''(x) + \frac{f'(x)\beta'(x)}{\beta(x)} \right) \int u^2 K(u) du,$$

shows how the bias is related to the regression function $f(x)$, as well as to the samples' distribution $\beta(x)$ [34], [35]. However, this asymptotic behavior is valid only for infinitesimal bandwidth, infinite samples ($h \rightarrow 0, nh \rightarrow \infty$) and requires the knowledge of the regression function and of the sampling distribution.

In a recent work, we propose an upper bound of the bias that is also valid for finite bandwidths [36]. We show under some Lipschitz conditions that the bound of the Nadaraya-Watson kernel regression bias does not depend on the samples' distribution, which is a desirable property in off-policy scenarios. The analysis is extended to multidimensional input space. For clarity of exposition, we report the main result in its simplest formulation, and later use it to infer the bound of the NPBE bias.

Theorem 2. *Let $f: \mathbb{R}^d \rightarrow \mathbb{R}$ be a Lipschitz continuous function with constant L_f . Assume a set $\{\mathbf{x}_i, y_i\}_{i=1}^n$ of i.i.d. samples from a log-Lipschitz distribution β with a Lipschitz constant L_β . Assume $y_i = f(\mathbf{x}_i) + \epsilon_i$, where $f: \mathbb{R}^d \rightarrow \mathbb{R}$ and ϵ_i is i.i.d. and zero-mean. The bias of the Nadaraya-Watson kernel regression with Gaussian kernels in the limit of infinite samples $n \rightarrow \infty$ is bounded by*

$$\left| \mathbb{E} \left[\lim_{n \rightarrow \infty} \hat{f}_n(\mathbf{x}) \right] - f(\mathbf{x}) \right| \leq \frac{L_f \sum_{k=1}^d \mathbf{h}_k \left(\prod_{i \neq k} \chi_i \right) \left(\frac{1}{\sqrt{2\pi}} + \frac{L_\beta \mathbf{h}_k}{2} \chi_k \right)}{\prod_{i=1}^d e^{-\frac{L_\beta^2 \mathbf{h}_i^2}{2}} \left(1 - \operatorname{erf} \left(\frac{\mathbf{h}_i L_\beta}{\sqrt{2}} \right) \right)},$$

where

$$\chi_i = e^{-\frac{L_\beta^2 \mathbf{h}_i^2}{2}} \left(1 + \operatorname{erf} \left(\frac{\mathbf{h}_i L_\beta}{\sqrt{2}} \right) \right),$$

$\mathbf{h} > 0 \in \mathbb{R}^d$ is the vector of bandwidths and erf is the error function.

Building on Theorem 2 we show that the solution of the NPBE is consistent with the solution of the true Bellman equation. Moreover, although the bound is not affected directly by $\beta(\mathbf{s})$, a smoother sample distribution $\beta(\mathbf{s})$ plays favorably in the bias term (a low L_β is preferred).

Theorem 3. *Consider an arbitrary MDP \mathcal{M} with a transition density p and a stochastic reward function $R(\mathbf{s}, \mathbf{a}) = r(\mathbf{s}, \mathbf{a}) + \epsilon_{\mathbf{s}, \mathbf{a}}$, where $r(\mathbf{s}, \mathbf{a})$ is a Lipschitz continuous function with L_R constant and $\epsilon_{\mathbf{s}, \mathbf{a}}$ denotes zero-mean noise. Assume $|R(\mathbf{s}, \mathbf{a})| \leq R_{\max}$ and a dataset D_n sampled from a log-Lipschitz distribution β defined over the state-action space with Lipschitz constant L_β . Let V_D be the unique solution of a nonparametric Bellman equation with Gaussian kernels ψ, φ, ϕ with positive bandwidths $\mathbf{h}_\psi, \mathbf{h}_\varphi, \mathbf{h}_\phi$ defined over the dataset $\lim_{n \rightarrow \infty} D_n$.*

Assume V_D to be Lipschitz continuous with constant L_V . The bias of such estimator is bounded by

$$|\bar{V}(\mathbf{s}) - V^*(\mathbf{s})| \leq \frac{1}{1 - \gamma_c} \left(A_{\text{Bias}} + \gamma_c L_V \sum_{k=1}^{d_s} \frac{h_{\phi, k}}{\sqrt{2\pi}} \right), \quad (9)$$

where $\bar{V}(\mathbf{s}) = \mathbb{E}_D[V_D(\mathbf{s})]$, A_{Bias} is the bound of the bias provided in Theorem 2 with $L_f = L_R$, $\mathbf{h} = [\mathbf{h}_\psi, \mathbf{h}_\varphi]$, $d = d_s + d_a$ and $V^*(\mathbf{s})$ is the fixed point of the ordinary Bellman equation.²

Theorem 3 shows that the value function provided by Theorem 1 is consistent when the bandwidth approaches infinitesimal values. Moreover, it is interesting to notice that the error can be decomposed in A_{Bias} , which is the bias component dependent on the reward's approximation, and the remaining term that depends on the smoothness of the value function and the bandwidth of ϕ , which can be read as the error of the transition's model.

The bound shows that smoother reward functions, state-transitions and sample distributions play favorably against the estimation bias. Notice that the bias persist even in the support points. This issue is known in Nadaraya-Watson kernel regression. However, the bias can be controlled and lowered by reducing the bandwidth. The i.i.d. assumption required by Theorem 3 is not restrictive, as even if the samples are collected by a sequential process that interacts with the MPD, the sample distribution will eventually converge to the stationary distribution of the MDP. Furthermore, our algorithm considers all the samples simultaneously, therefore, some inter-correlations between samples does not affect the estimation.

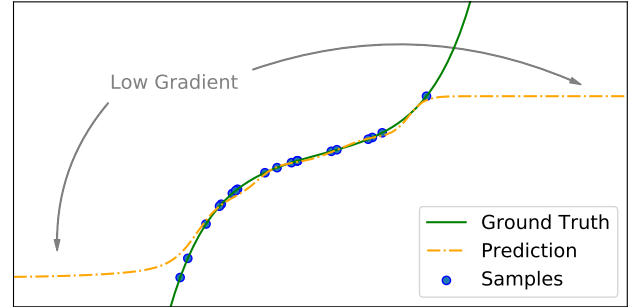


Fig. 2: The classic effect (known as boundary-bias) of the Nadaraya-Watson regression predicting a constant function in low-density regions is beneficial in our case, as it prevents the policy from moving in those areas as the gradient gets close to zero.

Beyond the bias analysis in the limit of infinite data is important to understand the variance and the bias for finite data. We provide a finite sample analysis in the empirical section. It is known that the lowest mean squared error is obtained by setting a higher bandwidth in presence of scarce data, and decreasing it with more data. In our implementation of NOPG, we select the bandwidth using cross validation.

² Complete proofs of the theorems and precise definitions can be found in the supplementary material.

3.3.1 A Trust Region

Very commonly, in order to prevent harmful policy optimization, the policy is constrained to stay close to the data [37], to avoid taking large steps [3], [38] or to circumvent large variance in the estimation [39], [40]. These techniques, which keep the policy updates in a trusted-region, prevent incorrect and dangerous estimates of the gradient. Even if we do not include any explicit constraint of this kind, the Nadaraya-Watson kernel regression automatically discourages policy improvements towards low-data areas. In fact, as depicted in Figure 2, the Nadaraya-Watson kernel regression, tends to predict a constant function in low density regions. Usually, this characteristic is regarded as an issue, as it causes the so-called boundary-bias. In our case, this effect turns out to be beneficial, as it constrains the policy to stay close to the samples, where the model is more correct.

4 RELATED WORK

Off-policy and offline policy optimization became increasingly more popular in the recent years and have been explored in many different flavors. Batch reinforcement learning, in the model-free view, has been elaborated both as a value-based and a policy gradient technique (we include actor-critic in this last class). Recently, offline reinforcement learning has been proposed also in the mode-based formulation. In this section, we aim to detail both the advantages and disadvantages of the proposed approaches. As we will see, our solution shares some advantages typical of the model-free policy gradient algorithms while using an approximated model of the dynamics and reward.

4.1 Model Free

The model-free offline formulation aims to improve the policy based purely on the samples collected in the dataset, without generating synthetic samples from an approximated model. We can divide this broad category in two main families: the value-based approaches, and the policy gradients.

4.1.1 Value Based

Value-based techniques are constructed on the approximate dynamic theory, leveraging on the policy-improvement theorem and on the contraction property of the Bellman operator. Examples of offline approximate dynamic programming algorithms are Fitted Q-Iteration (FQI) and Neural FQI (NFQI) [4], [5]. The max operator used in the optimal Bellman operator, usually restricts the applicability to discrete action spaces (few exceptions, [41]). Furthermore, the projected error can prevent the convergence to a satisfying solution [6]. These algorithms usually suffer also of the delusion bias [7]. Despite these issues, there has been a recent revival of value-based techniques in the context of offline reinforcement learning. Batch-Constrained Q-learning (BCQ) [12], at the best of our knowledge, firstly defined the extrapolation error, which is partially caused by optimizing unseen (out of distribution, OOD) state-action pairs in the dataset. This source of bias has been extensively studied in subsequent works, both in the model-free and model-based setting. Value-based methods using non-parametric

kernel-based approaches have also been used [26], [27], [42]. An interesting discussion in [29] shows that kernelized least square temporal difference approaches are also approximating the reward and transition models, and therefore they can be considered model-based.

4.1.2 Policy Gradient

This class of algorithms leverages their theory on the policy gradient theorem [10], [23]. Examples of policy gradients are REINFORCE [24], G(PO)MDP [43], natural policy gradient [44], and Trust-Region Policy Optimization (TRPO) [3]. Often, these approaches make use of approximate dynamic programming to estimate the Q -function (or related quantities), to obtain lower variance [2], [11], [38], [45]. The policy gradient theorem, however, defines the policy gradient w.r.t. *on-policy samples*. To overcome this problem two main techniques have been introduced: semi-gradient approaches, which rely on the omission of one term in the computation of the gradient, introduce an irreducible source of bias, while importance sampling solutions, which are unbiased, suffer from high variance.

Semi-Gradient: The off-policy policy gradient theorem was the first proposed off-policy actor-critic algorithm [9]. Since then, it has been used by the vast majority of state-of-the-art off-policy algorithms [2], [10], [11]. Nonetheless, it is important to note that this theorem and its successors, introduce two approximations to the original policy gradient theorem [23]. First, semi-gradient approaches consider a modified discounted infinite-horizon return objective $\hat{J}_\pi = \int \rho_\beta(\mathbf{s}) V_\pi(\mathbf{s}) d\mathbf{s}$, where $\rho_\beta(\mathbf{s})$ is state distribution under the behavioral policy π_β . Second, the gradient estimate is modified to be

$$\begin{aligned} \nabla_\theta \hat{J}_\pi &= \nabla_\theta \int_S \rho_\beta(\mathbf{s}) V_\pi(\mathbf{s}) d\mathbf{s} \\ &= \nabla_\theta \int_S \rho_\beta(\mathbf{s}) \int_A \pi_\theta(\mathbf{a}|\mathbf{s}) Q_\pi(\mathbf{s}, \mathbf{a}) d\mathbf{a} d\mathbf{s} \\ &= \int_S \rho_\beta(\mathbf{s}) \int_A \underbrace{\nabla_\theta \pi_\theta(\mathbf{a}|\mathbf{s}) Q_\pi(\mathbf{s}, \mathbf{a})}_{\text{A}} d\mathbf{a} d\mathbf{s} \\ &\quad + \underbrace{\pi_\theta(\mathbf{a}|\mathbf{s}) \nabla_\theta Q_\pi(\mathbf{s}, \mathbf{a})}_{\text{B}} d\mathbf{a} d\mathbf{s} \quad (10) \\ &\approx \int_S \rho_\beta(\mathbf{s}) \int_A \nabla_\theta \pi_\theta(\mathbf{a}|\mathbf{s}) Q_\pi(\mathbf{s}, \mathbf{a}) d\mathbf{a} d\mathbf{s}, \end{aligned}$$

where the term B related to the derivative of Q_π is ignored. The authors provide a proof that this biased gradient, or *semi-gradient*, still converges to the optimal policy in a tabular setting [8], [9]. However, further approximation (e.g., given by the critic and by finite sample size), might disallow the convergence to a satisfactory solution. Although these algorithms work correctly sampling from the replay memory (which discards *the oldest* samples), they have shown to fail with samples generated via a completely different process [8], [12]. The source of bias introduced in the semi-gradient estimation depends fully on the distribution mismatch, and cannot be recovered by an increment of the dataset size or with a more powerful function approximator. Still, mainly due to its simplicity, semi-gradient estimation has been used in the off-line scenario. The authors of these works do not tackle the distribution

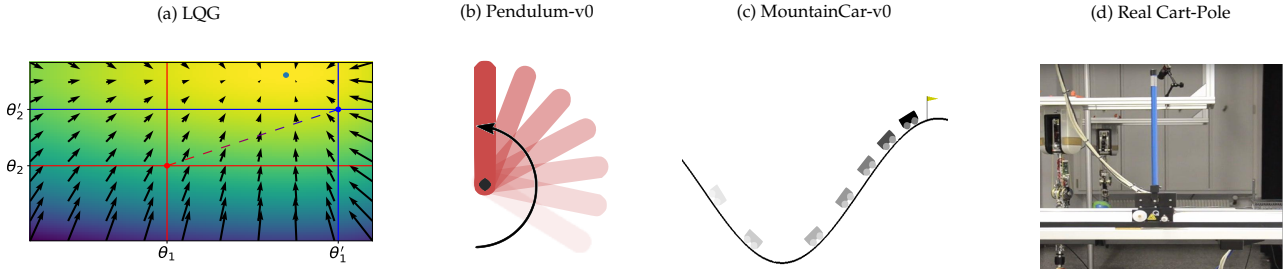


Fig. 3: Some of the benchmarking tasks. The return’s landscape (a) of the LQG problem. In the gradient analysis, we obtain the gradient of the policy with parameters θ_1, θ_2 by sampling from a policy interpolated with the parameters θ'_1, θ'_2 . Sub-figures (b) and (d) depicts the OpenAI environment used. The real system in (c) has been used to evaluate the policy learned to stabilize the cart-pole task.

mismatch with its impact to the gradient estimation, but rather consider to prevent the policy taking OOD actions. In this line of thoughts, Batch-Constrained Q-learning (BCQ) [12] introduces a regularization that keeps the policy close to the behavioral policy, Bootstrapping Error Accumulation Reduction (BEAR) [14] considers instead a pessimistic estimate of the Q function which penalizes the uncertainty, Behavior Regularized Actor Critic (BRAC) [15] proposes instead a generalization of the aforementioned approaches.

Importance-Sampling: One way to obtain an unbiased estimate of the policy gradient in an off-policy scenario is to re-weight every trajectory via importance sampling [16]–[18]. An example of the gradient estimation via G(PO)MDP [43] with importance sampling is given by

$$\nabla_{\theta} J_{\pi} = \mathbb{E} \left[\sum_{t=0}^{T-1} \rho_t \left(\prod_{j=0}^{t-1} \gamma_j \right) r_t \sum_{i=0}^t \nabla_{\theta} \log \pi_{\theta}(\mathbf{a}_i | \mathbf{s}_i) \right], \quad (11)$$

where $\rho_t = \prod_{z=0}^t \pi_{\theta}(\mathbf{a}_z | \mathbf{s}_z) / \pi_{\beta}(\mathbf{a}_z | \mathbf{s}_z)$. This technique applies only to stochastic policies and requires the knowledge of the behavioral policy π_{β} . Moreover, Equation (11) shows that path-wise importance sampling (PWIS) needs a trajectory-based dataset, since it needs to keep track of the past in the correction term ρ_t , hence introducing more restrictions on its applicability. Additionally, importance sampling suffers from high variance [46]. Recent works have helped to make PWIS more reliable. For example, [8], building on the emphatic weighting framework [47], proposed a trade-off between PWIS and semi-gradient approaches. Another possibility consists in restricting the gradient improvement to a safe-region, where the importance sampling does not suffer from too high variance [39]. Another interesting line of research is to estimate the importance sampling correction on a state-distribution level instead of on the classic trajectory level [48]–[50]. We note that despite the nice theoretical properties, all these promising algorithms have been applied on low-dimensional problems, as importance sampling suffers from the curse of dimensionality.

4.2 Model-Based

While all model-free offline techniques rely purely on the samples contained in the offline dataset, model-based tech-

niques aim to approximate the transitions from that dataset. The approximated model is then used to generate new artificial samples. These approaches do not suffer from the distribution mismatch problem described above, as the samples can be generated on-policy by the model (and therefore, in principle, any online algorithm can be used). This advantage is overshadowed by the disadvantage of having unrealistic trajectories generated by the approximated model. For this reason, many recent works focus on discarding unrealistic samples, relying on a pessimistic approach towards uncertainty. In some sense, we encounter again the problem of quantifying our uncertainty - given the limited information contained in the dataset - and to prevent the policy or the model to use or generate uncertain samples. In this view, the Probabilistic Ensemble with Trajectory Sampling (PETS) [40] uses an ensemble of probabilistic models of the dynamics to quantify both the epistemic and the aleatoric uncertainties, and uses model predictive control to act in the real environment. Model Based Offline Planning (MBOP) [51] uses a behavioral cloning policy as a prior to the planning algorithm. Plan Online and Learn Offline (POLO) [52] proposes to learn the value function from a known model of the dynamics and to use model predictive control on the environment. Both Model Based Reinforcement Learning (MOReL) [20] and Model-based Offline Policy Optimization (MOPO) [19] learn instead the model to train a parametric policy. MOReL learns a pessimistic version of the real MDP, by partitioning the state-action space in known and unknown and penalizing the policies visiting the unknown region. Instead, MOPO builds a pessimistic MDP by introducing a reward penalization toward model uncertainty.

NOPG, instead, provides a theoretical framework built on a nonparametric approximation of the reward and the state transition. Such approximation is used to compute the policy gradient in closed-form. For this reason, our method differs from classic model-based solutions since it does not generate synthetic trajectories. Most of the state-of-the-art model-free offline algorithms, on the other hand, utilize a biased and inconsistent gradient estimate. Instead, our approach delivers a full-gradient estimate that allows a trade-off between bias and variance. The quality of the gradient estimate results in a particularly sample-efficient

policy optimization, as seen in the empirical section.

5 EMPIRICAL EVALUATION

In this section, we analyze our method. Therefore, we divide our experiments in two: the analysis of the gradient, and the analysis of the policy optimization using a gradient ascent technique. The analysis of the gradient comprises an empirical evaluation of the bias, the variance and the gradient direction w.r.t. the ground truth, in relation to some quantities such as the size of the dataset or its degree of “off-policiness”. In the policy optimization analysis, instead, we aim to both compare the sample efficiency of our method in comparison to state-of-the-art policy gradient algorithms, and to study its applicability to unstructured and human-demonstrated datasets.

5.1 Benchmarking Tasks

In the following, we give a brief description of the tasks involved in the empirical analysis.

5.1.1 Linear Quadratic Gaussian Controller

A very classical control problem consists of linear dynamics, quadratic reward and Gaussian noise. The main advantage of this control problem relies in the fact that it is fully solvable in closed-form, using the Riccati equations, which makes it appropriate for verifying the correctness of our algorithm. In our specific scenario, we have a policy encoded with two parameters for illustration purposes. The LQG is defined as

$$\begin{aligned} & \max_{\theta} \sum_{t=0}^{\infty} \gamma^t r_t \\ \text{s.t. } & \mathbf{s}_{t+1} = A\mathbf{s}_t + B\mathbf{a}_t; \quad r_t = -\mathbf{s}_t^T Q \mathbf{s}_t - \mathbf{a}_t^T R \mathbf{a}_t \\ & \mathbf{a}_{t+1} = \Theta \mathbf{s}_t + \Sigma \epsilon_t; \quad \epsilon_t \sim \mathcal{N}(0, I), \end{aligned}$$

with A, B, Q, R, Σ diagonal matrix and $\Theta = \text{diag}(\theta)$ where θ are considered the policy’s parameters. In the stochastic policy experiments, $\pi_{\theta}(\mathbf{a}|\mathbf{s}) = \mathcal{N}(\mathbf{a}|\Theta\mathbf{s}; \Sigma)$, while for the deterministic case $\Sigma = \mathbf{0}$ and $\pi_{\theta}(\mathbf{s}) = \Theta\mathbf{s}$. For further details, please refer to the supplementary material.

5.1.2 OpenAI Pendulum-v0

The OpenAI Pendulum-v0 [53] is a popular benchmark in reinforcement learning. It simulates a simple under-actuated inverted-pendulum. The goal is to swing the pendulum until it reaches the top position, and then to keep it stable. The state of the system is fully described by the angle of the pendulum ω and its angular velocity $\dot{\omega}$. The applied torque $\tau \in [-2, 2]$ corresponds to the agent’s action. One of the advantages of such a system, is that its well-known value function is two-dimensional.

5.1.3 Quanser Cart-pole

The cart-pole is another classical task in reinforcement learning. It consists of an actuated cart moving on a track, to which a pole is attached. The goal is to actuate the cart in a way to balance the pole in the top position. Differently from the inverted pendulum, the system has a further degree of complexity, and the state space requires the position on the track x , the velocity of the cart \dot{x} , the angle of the pendulum ω and its angular velocity $\dot{\omega}$.

| Acronym | Description | Typology |
|-------------|--|----------|
| NOPG-D | Our method with deterministic policy. | NOPG |
| NOPG-S | Our method with stochastic policy. | |
| G(PO)MDP+N | G(PO)MDP with normalized importance sampling. | PWIS |
| G(PO)MDP+BN | G(PO)MDP with normalized importance sampling and generalized baselines. | |
| DPG+Q | Offline version of the deterministic policy gradient theorem with an oracle for the Q -function. | SG |
| DDPG | Deep Deterministic Policy Gradient. | |
| TD3 | Improved version of DDPG. | |
| SAC | Soft Actor Critic. | |
| BEAR | Bootstrapping Error Accumulation Reduction. | |
| BRAC | Behavior Regularized Actor Critic. | |
| MOPO | Model-based Offline Policy Optimization. | MB |
| MOREL | Model-Based Offline Reinforcement Learning. | |

TABLE 1: Acronyms used in the paper to refer to practical implementation of the algorithms (SG: semi-gradient, PWIS: path-wise importance sampling, MB: model based).

5.1.4 OpenAI Mountain-Car

The mountain-car (also known as car-on-hill), consists on an under-powered car that must reach the top of a hill. The car is placed in the valley connecting two hills. In order to reach the goal position, it must first go in opposite direction in order to gain momentum. Its state is described by the x -position of the car, and by its velocity \dot{x} . The episodes terminate when the car reaches the goal. In contrast to the swing-up pendulum, which is hardly controllable by a human-being, this car system is ideal to provide human-demonstrated data.

5.1.5 U-Maze

U-Maze is an environment from the D4RL dataset [54]. It consist of a simple maze with a 2d shape, where a ball should reach a goal position. The state representation is 4-dimensional (2d position and velocity), and the 2d action represents the velocity of the ball.

5.1.6 Hopper

The Hopper is a popular one-legged robot, with 11-dimensional state and 3-dimensional action space, that should hop forward as fast as possible in a two-dimensional world. We use the implementation offered by MuJoCo [55]. Also in this case, we test NOPG on a dataset provided by D4RL.

5.2 Algorithms Used for Comparisons

To provide an analysis of the gradient, we compare our algorithm against G(PO)MDP with importance sampling, and with offline DPG (DPG with fixed dataset). Instead of using the naïve form of G(PO)MDP with importance sampling, which suffers from high variance, we used the normalized importance sampling [56], [57] (which introduces some bias but drastically reduces the variance), and the generalized baselines [58] (which also introduce some bias, as they are

estimated from the same dataset). The offline version of DPG, suffers from three different sources of bias: the semi-gradient, the critic approximation and the improper use of the discounted state distribution [59], [60]. To mitigate these issues and focus more on the semi-gradient contribution to the bias, we provide an oracle Q -function (we denote this version as DPG+Q). For the policy improvement, instead, we compare both with online algorithms (Figure 9) such as TD3 [12] and SAC [2], and with offline algorithms (BEAR [14], BRAC [15], MOPO [19] and MOREL [20]) as depicted in Figure 10. A full list of the algorithms used in the comparisons with a brief description is available in Table 1.

5.3 Analysis of the Gradient

We want to compare the bias and variance of our gradient estimator w.r.t. the already discussed classical estimators. Therefore, we use the LQG setting described in Section 5.1.1, which allows us to compute the true gradient. Our goal is to estimate the gradient w.r.t. the policy π_θ diagonal parameters θ_1, θ_2 , while sampling from a policy which is a linear combination of Θ and Θ' . The hyper-parameter α determines the mixing between the two parameters. When $\alpha = 1$ the behavioral policy will have parameters Θ' , while when $\alpha = 0$ the dataset will be sampled using Θ . In Figure 4, we can visualize the difference of the two policies with parameters Θ and Θ' . Although not completely disjoint, they are fairly far in the probability space, especially if we take into account that such distance propagates in the length of the trajectories.

5.3.1 Sample Analysis

We want to study how the bias, the variance and the direction of the estimated gradient vary w.r.t. the dataset's size. We are particularly interested in the off-policy strategy for sampling, and in this set of experiments we will use constant $\alpha = 0.5$. Figure 6a depicts these quantities w.r.t. the number of collected samples. As expected, a general trend for all algorithms is that with a higher number of samples we are able to reduce the variance. The importance sampling based G(PO)MDP algorithms eventually obtain a low bias as well. Remarkably, NOPG has significantly both lower

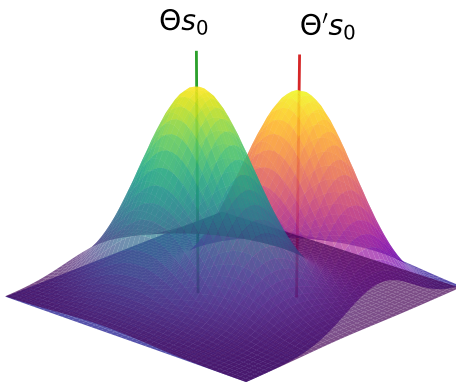


Fig. 4: Evaluated in the initial state, the optimization policy having parameters θ_1, θ_2 and the behavioral policy having parameters θ'_1, θ'_2 exhibit a fair distance in probability space.

bias and variance, and its gradient direction is also more accurate w.r.t. the G(PO)MDP algorithms (note the different scales of the y-axis). Between DPG+Q and NOPG there is no sensible difference, but we should take into account the already-mentioned advantage of DPG+Q to have access to the true Q -function.

5.3.2 Off-Policy Analysis

We want to estimate the bias and the variance w.r.t. different degrees of “off-policiness” α , as defined in the beginning of Section 5.3. We want to highlight that in the deterministic experiment the behavioral policy remains stochastic. This is needed to ensure the stochastic generation of datasets, which is essential to estimate the bias and the variance of the estimator. As depicted in Figure 6, the variance in importance sampling based techniques tends to increase when the dataset is off-policy. On the contrary, NOPG seems to be more subject to an increase of bias. This trend is also noticeable in DPG+Q, where the component of the bias is the one playing a major role in the mean squared error. The gradient direction of NOPG seems however unbiased, while DPG+Q has a slight bias but remarkably less variance (note the different scales of the y-axis). We remark that DPG+Q uses an oracle for the Q -function, which supposedly results in lower variance and bias³. The positive bias of DPG+Q in the on-policy case ($\alpha = 0$) is caused by the improper use of discounting. In general, NOPG shows a decrease in bias and variance in order of magnitudes when compared to the other algorithms.

5.3.3 Bandwidth Analysis

In the previous analysis, we kept the bandwidth's parameters of our algorithm fixed, even though a dynamic adaptation of this parameter w.r.t. the size of the dataset might have improved the bias/variance trade-off. We are now interested in studying how the bandwidth impacts the gradient estimation. For this purpose, we generated datasets of 1000 samples with $\alpha = 0.5$. We set all the bandwidths of state, action and next state, for each dimension equal to κ . From Figure 8, we evince that a lower bandwidth corresponds to a higher variance, while a larger bandwidth approaches a constant bias and the variance tends to zero. This result is in line with the theory.

5.3.4 Trust Region

In Section 3.3.1, we claimed that the nonparametric technique used has the effect to not consider OOD actions, and more in general, state-action pairs that are in a low density region: in fact the magnitude of the gradient in these regions is low. To appreciate this effect, we considered the Pendulum-v0. We generated the data using a Gaussian policy $\mathcal{N}(\mu = 0, \Sigma = 0.2I)$. Figure 5a depicts the generated dataset. Subsequently, we generated a set of linear policies $\mathbf{a} = \theta_0 \sin \omega + \theta_1 \cos \omega + \theta_2 \dot{\omega} + \theta_3$ where the parameters $\theta_0 = \theta_1 = \theta_2 = 0, \theta_3 \in [-2, 2]$ and ω and $\dot{\omega}$ represent the angle and the angular velocity of the pendulum. When θ_3

3. Furthermore, we suspect that the particular choice of a LQG task tends to mitigate the problems of DPG, as the fast convergence to a stationary distribution due to the stable attractor, united with the improper discounting, results in a coincidental correction of the state-distribution.

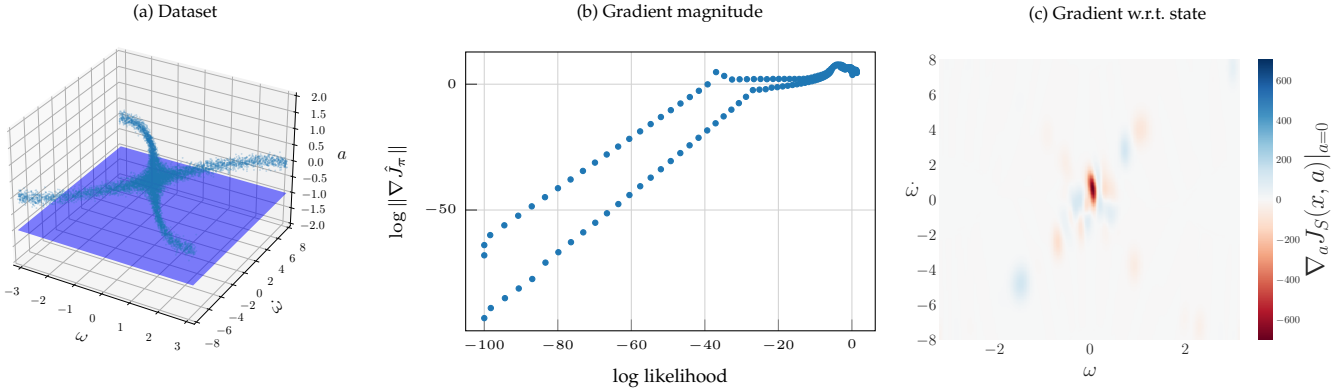


Fig. 5: (a) The dataset used for the experiment in Section 5.3.4. The blue plane represent a policy with constant action. By setting different values of θ_3 we can obtain different policies. For $\theta_3 \approx 0$, the policy is most fitting with the data. (b) When the policy has low log-likelihood, the gradient quickly approaches the zero (i.e., $\|\nabla_{\theta} \hat{J}_\pi\| \rightarrow 0$). (c) The magnitude of the gradient decreases in low density regions, where the prediction is most uncertain.

is close to 0, the policy is close to the samples contained in the data, while if θ_3 is close either to -2 or 2 , then it is more distant. In Figure 5b shows the estimated policy gradient for different policies. In particular, each point represents the log-likelihood of the policy (w.r.t. the actions contained in the dataset) on the x -axis, and the logarithm of the magnitude of the gradient on the y -axis. There is a clear correlation between the log-likelihood and the magnitude of the gradient, which tells us that the gradient is close to zero for unlikely policies, supporting, therefore, our claim. Furthermore, we investigate the contribution of the single state-action pairs to the gradient. The heatmap in Figure 5c shows that the highest gradient magnitude appears on the diagonals of the state space. Looking at the generated data, in Figure 5a, we notice that the majority of samples are also present on the aforementioned diagonals forming a “X” shape. Hence, our experiment shows that the magnitude of the gradient depends also on the density of the state-action space, with lower magnitude in correspondence of lower density of the state space.

5.4 Policy Improvement

In the previous section, we analyzed the statistical properties of our estimator. Conversely, in this section, we use the NOPG estimate to fully optimize the policy. At the current state, NOPG is a batch algorithm, meaning that it receives as input a set of data, and it outputs an optimized policy, without any interaction with the environment. We study the sample efficiency of the overall algorithm. We compare it with both other batch and online algorithms. Please notice that online algorithms, such as DDPG-On, TD3 and SAC, can acquire more valuable samples during the optimization process. Therefore, in a direct comparison, batch algorithms are in disadvantage.

5.4.1 Uniform Grid

In this experiment we analyze the performance of NOPG under a uniformly sampled dataset, since, as the theory suggests, this scenario should yield the least biased estimate of NOPG. We generate datasets from a grid over

the state-action space of the pendulum environment with different granularities. We test our algorithm by optimizing a policy encoded with a neural-network for a fixed amount of iterations. The policy is composed of a single hidden layer with 50 neurons and ReLU activations. This configuration is fixed across all the different experiments and algorithms for the remainder of this document. The resulting policy is evaluated on trajectories of 500 steps starting from the bottom position. The leftmost plot in Figure 9, depicts the performance against different dataset sizes, showing that NOPG is able to solve the task with 450 samples. Figure 7 is an example of the value function and state distribution estimates of NOPG-D at the beginning and after 300 optimization steps. The ability to predict the state-distribution is particularly interesting for robotics, as it is possible to predict in advance whether the policy will move towards dangerous states. Note that this experiment is not applicable to PWIS, as it does not admit non-trajectory-based data.

5.4.2 Comparison with Online Algorithms

In contrast to the uniform grid experiment, here we collect the datasets using trajectories from a random agent in the pendulum and the cart-pole environments. In the pendulum task, the trajectories are generated starting from the upright position and applying a policy composed of a mixture of two Gaussians. The policies are evaluated starting from the bottom position with an episode length of 500 steps. The datasets used in the cart-pole experiments are collected using a uniform policy starting from the upright position until the end of the episode, which occurs when the absolute value of the angle θ surpasses 3 deg. The optimization policy is evaluated for 10^4 steps. The reward is $r_t = \cos \theta_t$. Since θ is defined as 0 in the top-right position, a return of 10^4 indicates an optimal policy behavior.

We analyze the sample efficiency by testing NOPG in an offline fashion with pre-collected samples, on a different number of trajectories. In addition, we provide the learning curve of DDPG, TD3 and SAC using the implementation in Mushroom [61]. For a fixed size of the dataset, we optimize DDPG-Off and NOPG for a fixed number of steps. For NOPG, which is offline, we select the policy from the

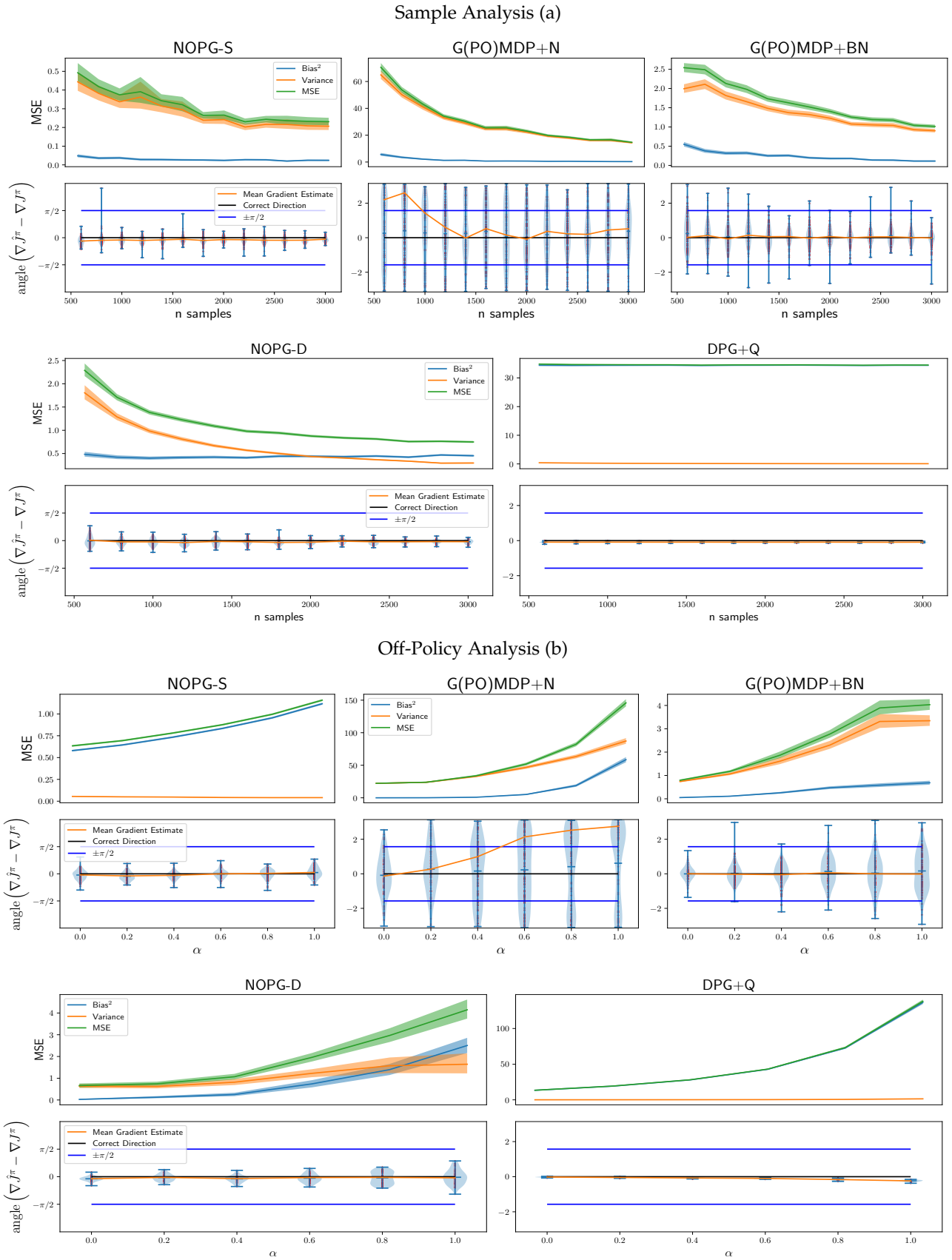


Fig. 6: Bias, variance, MSE and gradient direction analysis. The MSE plots are equipped with a 95% interval using bootstrapping techniques. The direction analysis plots describe the distribution of angle between the estimates and the ground truth gradient. NOPG exhibits favorable bias, variance and gradient direction compared to PWIS and semi-gradient.

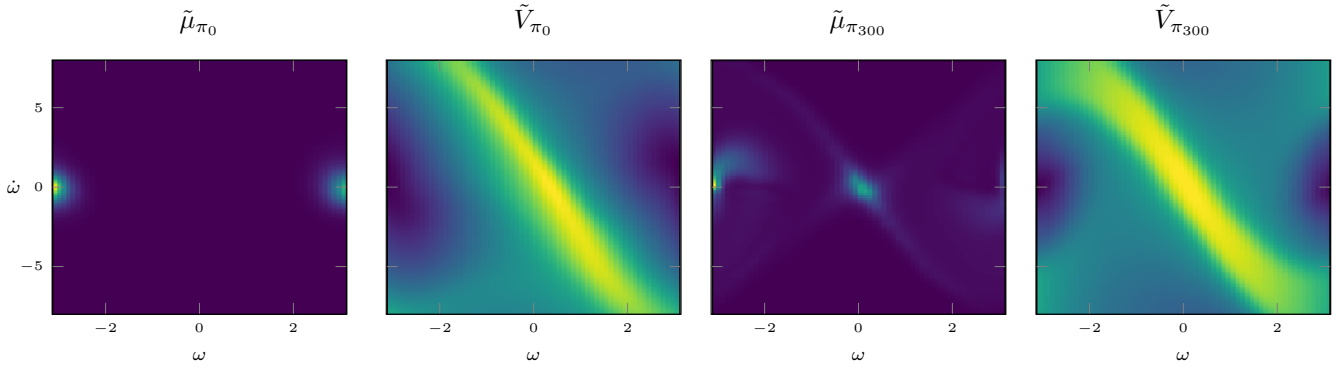


Fig. 7: A phase portrait of the state distribution $\tilde{\mu}_{\pi}$ and value function \tilde{V}_{π} estimated in the swing-up pendulum task with NOPG-D. Green corresponds to higher values. The two leftmost figures show the estimates before any policy improvement, while the two rightmost show them after 300 offline updates of NOPG-D. Notice that the algorithm finds a very good approximation of the optimal value function and is able to predict that the system will reach the goal state $((\omega, \dot{\omega}) = (0, 0))$.

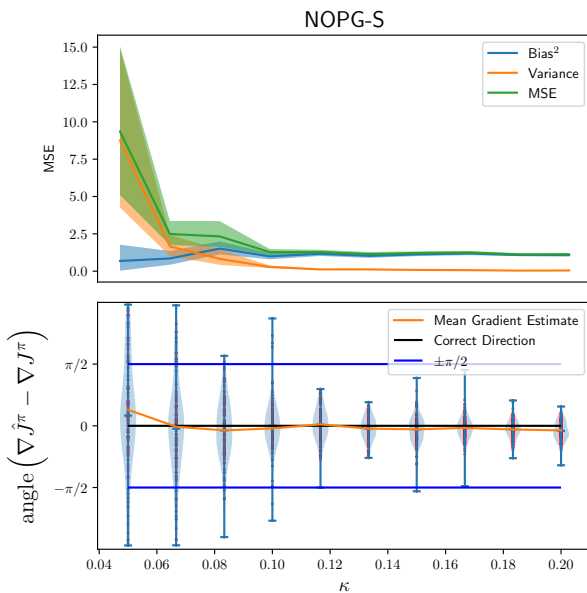


Fig. 8: A lower bandwidth corresponds to higher variance, while higher bandwidth increases the bias up to a plateau.

last optimization step. The two rightmost plots in Figure 9 highlight that our algorithm has superior sample efficiency by more than one order of magnitude w.r.t. the considered online algorithms (note the log-scale on the x-axis).

To validate the resulting policy learned in the simulated cartpole (Figure 3), we apply the final learned controller on a real Quanser cart-pole, and observe a successful stabilizing behavior as can be seen in the supplementary video.

5.4.3 Comparison with Offline Algorithms

We use the same environments provided in Section 5.4.2 to compare against state-of-the-art offline algorithms. To this end, we used the same datasets on Cart-Pole and Pendulum-v0 to train BRAC, BEAR, MOPO and MOREL. Furthermore, to allow a fairer comparison using the D4RL dataset, we tested our algorithm with the aforementioned baselines on the U-Maze. To perform the usual sample-analysis, we

sub-sampled the dataset in smaller datasets. The results of such analysis can be viewed in Figure 10. NOPG exhibits a competitive performance w.r.t. the baselines. In more detail, BEAR and MOREL perform suboptimally in our experiments, MOPO perform similarly to NOPG in Pendulum-v0, while failing in Quanser Cart-Pole. BRAC exhibit a similar behavior with our NOPG. All the algorithms seems, however, to fail with the U-Maze, probably due to the scarcity of data, and due to its sparse reward.

5.4.4 Human Demonstrated Data

In robotics, learning from human demonstrations is crucial in order to obtain better sample efficiency and to avoid dangerous policies. This experiment is designed to showcase the ability of our algorithm to deal with such demonstrations without the need for explicit knowledge of the underlying behavioral policy. The experiment is executed in a completely offline fashion after collecting the human dataset, i.e., without any further interaction with the environment. This setting is different from the classical imitation learning and subsequent optimization [62]. As an environment we choose the continuous mountain car task from OpenAI. We provide 10 demonstrations recorded by a human operator and assigned a reward of -1 to every step. A demonstration ends when the human operator surpasses the limit of 500 steps, or arrives at the goal position. The human operator explicitly provides sub-optimal trajectories, as we are interested in analyzing whether NOPG is able to take advantage of the human demonstrations to learn a better policy than that of the human, without any further interaction with the environment. To obtain a sample analysis, we evaluate NOPG on randomly selected subsets of the trajectories from the human demonstrations. Figure 11 shows the average performance as a function of the number of demonstrations as well as an example of a human-demonstrated trajectory. A vanilla behavioral cloning approach trained with the whole dataset leads to a worse performance w.r.t. the human demonstrator. In fact, by simply replicating the demonstrator, the cloned behavior is most of the times not able to reach the flag. Notice that both NOPG-S and NOPG-D manage to learn a policy that

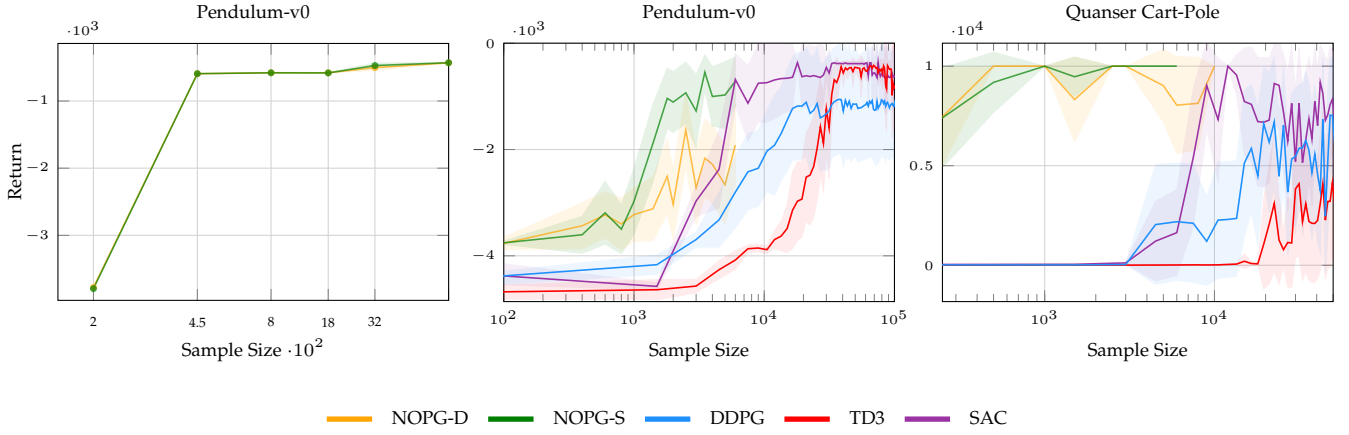


Fig. 9: Comparison of NOPG in its deterministic and stochastic versions to state-of-the-art **online** algorithms on continuous control tasks: Swing-Up Pendulum with **uniform grid** sampling (left), Swing-Up Pendulum with the **random agent** (center) and the Cart-Pole stabilization (right). The figures depict the mean and 95% confidence interval over 10 trials. NOPG outperforms the baselines w.r.t the sample complexity. **Note the log-scale along the x -axis.**

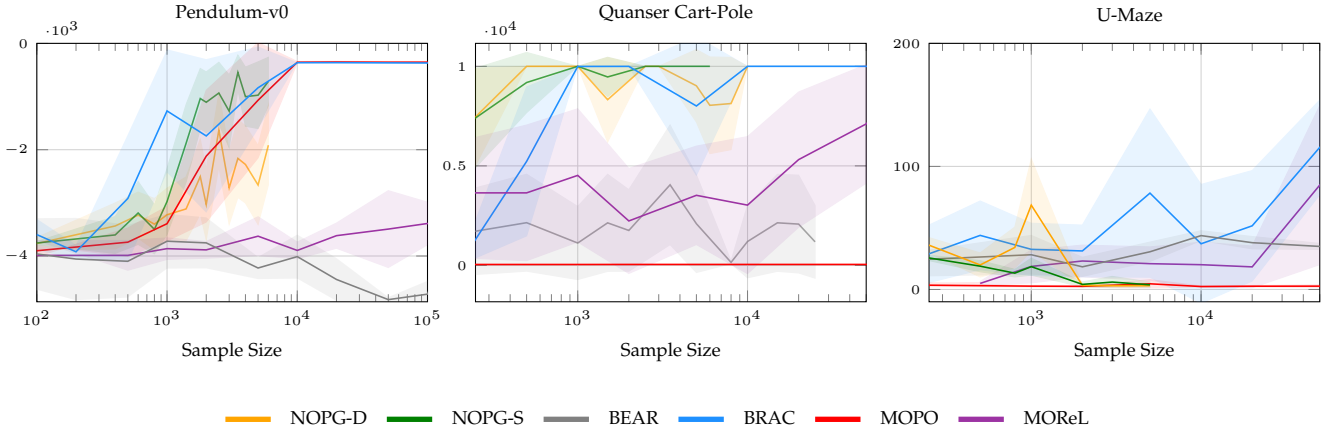


Fig. 10: Comparison of NOPG in its deterministic and stochastic versions to state-of-the-art **offline** algorithms on continuous control tasks: Swing-Up Pendulum with **random agent** (left), the Cart-Pole stabilization (center) and U-Maze with D4RL dataset (right). The figures depict the mean and 95% confidence interval over 10 trials. NOPG is competitive with the sample efficiency of the considered baselines. **Note the log-scale along the x -axis.**

surpasses the human operator’s performance and reach the optimal policy with two demonstrated trajectories.

5.4.5 Test on a Higher-Dimension Task

All the considered tasks, are relatively low dimensional, with the higher-dimension of 6, accounting for both states and actions, in the U-Maze. We tested NOPG also on the Hopper, using the D4RL dataset. NOPG improves w.r.t. the number of samples provided, although it does not reach a satisfactory policy (Figure 12). The low performance is probably caused by the poor scaling to high dimensions of nonparametric methods, and the typical need of a large amount of samples due to the complexity of the considered task.

5.5 Computational Complexity

Our nonparametric approach involves a layer of computation that is not usual in classic deep reinforcement learning solutions. In particular, the construction of the matrix $\hat{\mathbf{P}}_{\pi}^{\gamma}$ and the inversion of $\mathbf{\Lambda}_{\pi}$ can be expensive. In the following,

we analyze the computational resources required by NOPG. In particular, we use different sizes of the Pendulum-v0 dataset and investigate the time required to compute an iteration of Algorithm 1. As stated in Section 3.2, the iteration time grows quadratically w.r.t. the number of samples contained in the dataset. The computational cost can be lowered by lowering the number of non-zero element of the matrix $\hat{\mathbf{P}}_{\pi}^{\gamma}$ (Figure 13). However, while our algorithm considers all the samples at every iteration, classic deep reinforcement learning algorithms usually consider only a fixed amount of data (called “mini batch”), and the computational cost of the iterations results, therefore, to be constant.

6 CONCLUSION AND FUTURE WORK

In this paper, we presented and analyzed an off-policy gradient technique *Nonparametric Off-policy Policy Gradient* (NOPG) [21]. Our estimator overcomes the main issues of the techniques of off-policy gradient estimation. On the one hand, in contrast to semi-gradient approaches, it delivers a full-gradient estimate; and on the other hand, it avoids

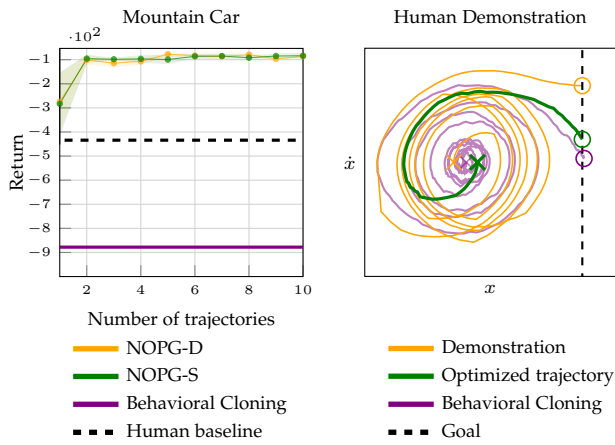


Fig. 11: With a small amount of data NOPG is able to reach a policy that surpasses the human demonstrator (dashed line) in the mountain car environment. Depicted are the mean and 95% confidence over 10 trials (left). An example of a human-demonstrated trajectory and the relative optimized version obtained with NOPG (right). Although the human trajectories in the dataset are suboptimal, NOPG converges to an optimal solution (right).

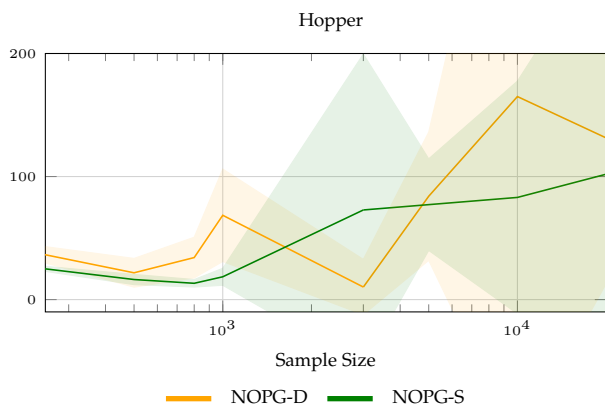


Fig. 12: Performance of NOPG on the Hopper-v0, using the D4RL dataset.

the high variance of importance sampling by phrasing the problem with nonparametric techniques. The empirical analysis clearly showed a better gradient estimate in terms of bias, variance, and direction. Our experiments also showed that our method has high sample efficiency and that our algorithm can be behavioral-agnostic and cope with unstructured data.

However, our algorithm, which is built on nonparametric techniques, suffers from the curse of dimensionality. The future work aims to mitigate this problem. We plan to investigate better sparsification techniques united with an adaptive bandwidth. The promising properties of the proposed gradient estimation can, in the future, be adapted to the parametric inference, to extend our approach to the more versatile deep-learning setting.

ACKNOWLEDGMENTS

The research is financially supported by the Bosch-Forschungsförderung program and the European Union's

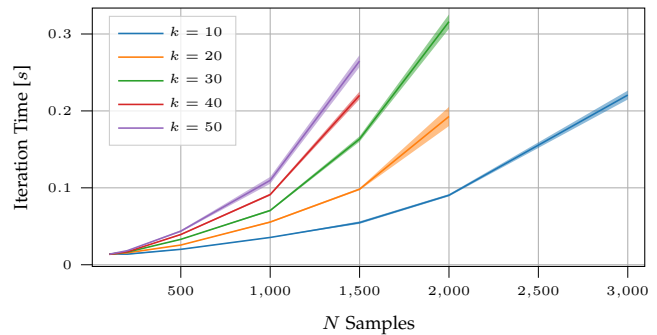


Fig. 13: For a fixed amount k of non-zero elements per row of the transition matrix, the iteration time grows quadratically w.r.t. the number of samples. A lower k requires a shorter iteration time.

Horizon 2020 research and innovation program under grant agreement #640554 (SKILLS4ROBOTS).

REFERENCES

- [1] V. Mnih, K. Kavukcuoglu, D. Silver, A. A. Rusu, J. Veness, M. G. Bellemare, A. Graves, M. Riedmiller, A. K. Fidjeland, G. Ostrovski, S. Petersen, C. Beattie, A. Sadik, I. Antonoglou, H. King, D. Kumaran, D. Wierstra, S. Legg, and D. Hassabis, "Human-Level Control Through Deep Reinforcement Learning," *Nature*, vol. 518, no. 7540, pp. 529–533, 2015. [Online]. Available: <http://www.nature.com/articles/nature14236>
- [2] T. Haarnoja, A. Zhou, P. Abbeel, and S. Levine, "Soft Actor-Critic: Off-Policy Maximum Entropy Deep Reinforcement Learning with a Stochastic Actor," in *Proceedings of the 35th International Conference on Machine Learning*, 2018, pp. 1856–1865.
- [3] J. Schulman, S. Levine, P. Moritz, M. Jordan, and P. Abbeel, "Trust Region Policy Optimization," in *Proceedings of the 32nd International Conference on Machine Learning*, 2015, pp. 1889–1897.
- [4] D. Ernst, P. Geurts, and L. Wehenkel, "Tree-Based Batch Mode Reinforcement Learning," *Journal of Machine Learning Research*, vol. 6, no. Apr, pp. 503–556, 2005. [Online]. Available: <http://www.jmlr.org/papers/v6/ernst05a.html>
- [5] M. Riedmiller, "Neural Fitted Q Iteration – First Experiences with a Data Efficient Neural Reinforcement Learning Method," in *European Conference of Machine Learning*, ser. Lecture Notes in Computer Science. Springer Berlin Heidelberg, 2005, pp. 317–328.
- [6] L. Baird, "Residual Algorithms: Reinforcement Learning with Function Approximation," *Machine Learning Proceedings*, pp. 30–37, 1995.
- [7] T. Lu, D. Schuurmans, and C. Boutilier, "Non-Delusional Q-learning and Value-Iteration," in *Advances in Neural Information Processing Systems*. Curran Associates, Inc., 2018, pp. 9949–9959. [Online]. Available: <http://papers.nips.cc/paper/8200-non-delusional-q-learning-and-value-iteration.pdf>
- [8] E. Imani, E. Graves, and M. White, "An Off-Policy Policy Gradient Theorem Using Emphatic Weightings," in *Advances in Neural Information Processing Systems*, 2018, pp. 96–106.
- [9] T. Degris, M. White, and R. S. Sutton, "Off-Policy Actor-Critic," *arXiv:1205.4839 [cs]*, May 2012, arXiv: 1205.4839. [Online]. Available: <http://arxiv.org/abs/1205.4839>
- [10] D. Silver, G. Lever, N. Heess, T. Degris, D. Wierstra, and M. Riedmiller, "Deterministic Policy Gradient Algorithms," in *Proceedings of the 31st International Conference on Machine Learning*, 2014.
- [11] T. P. Lillicrap, J. J. Hunt, A. Pritzel, N. Heess, T. Erez, Y. Tassa, D. Silver, and D. Wierstra, "Continuous Control with Deep Reinforcement Learning," in *International Conference on Learning Representations*, 2016, arXiv: 1509.02971. [Online]. Available: <http://arxiv.org/abs/1509.02971>
- [12] S. Fujimoto, D. Meger, and D. Precup, "Off-Policy Deep Reinforcement Learning without Exploration," in *Proceedings of the 36th International Conference on Machine Learning*, 2019, pp. 2052–2062. [Online]. Available: <http://proceedings.mlr.press/v97/fujimoto19a/fujimoto19a.pdf>

- [13] A. Kumar, A. Zhou, G. Tucker, and S. Levine, "Conservative Q-Learning for Offline Reinforcement Learning," *arXiv preprint arXiv:2006.04779*, 2020.
- [14] A. Kumar, J. Fu, G. Tucker, and S. Levine, "Stabilizing Off-Policy Q-Learning via Bootstrapping Error Reduction," *arXiv preprint arXiv:1906.00949*, 2019.
- [15] Y. Wu, G. Tucker, and O. Nachum, "Behavior Regularized Offline Reinforcement Learning," *arXiv preprint arXiv:1911.11361*, 2019.
- [16] C. R. Shelton, "Policy Improvement for POMDPs Using Normalized Importance Sampling," in *Proceedings of the Seventeenth Conference on Uncertainty in Artificial Intelligence*, ser. UAI'01. Morgan Kaufmann Publishers Inc., 2001, pp. 496–503, event-place: Seattle, Washington. [Online]. Available: <http://dl.acm.org/citation.cfm?id=2074022.2074083>
- [17] N. Meuleau, L. Peshkin, and K.-E. Kim, "Exploration in Gradient-Based Reinforcement Learning," Massachusetts Institute of Technology, Tech. Rep., 2001. [Online]. Available: <https://dspace.mit.edu/handle/1721.1/6076>
- [18] L. Peshkin and C. R. Shelton, "Learning from Scarce Experience," in *Proceedings of the Nineteenth International Conference on Machine Learning*, 2002, arXiv: cs/0204043. [Online]. Available: <http://arxiv.org/abs/cs/0204043>
- [19] T. Yu, G. Thomas, L. Yu, S. Ermon, J. Zou, S. Levine, C. Finn, and T. Ma, "MOPO: Model-based Offline Policy Optimization," in *Proceedings of the 33rd International Conference on Neural Information Processing Systems*, 2020.
- [20] R. Kidambi, A. Rajeswaran, P. Netrapalli, and T. Joachims, "MOREL: Model-based Offline Reinforcement Learning," *arXiv preprint arXiv:2005.05951*, 2020.
- [21] S. Tosatto, J. Carvalho, H. Abdulsamad, and J. Peters, "A Non-parametric Off-Policy Policy Gradient," in *Proceedings of the 23rd International Conference on Artificial Intelligence and Statistics (AISTATS)*, S. Chiappa and R. Calandra, Eds., Palermo, Italy, 2020.
- [22] M. White, "Unifying Task Specification in Reinforcement Learning," in *Proceedings of the 34th International Conference on Machine Learning*. JMLR.org, 2017, pp. 3742–3750.
- [23] R. S. Sutton, D. A. McAllester, S. P. Singh, and Y. Mansour, "Policy Gradient Methods for Reinforcement Learning with Function Approximation," in *Advances in Neural Information Processing Systems*, 2000, pp. 1057–1063.
- [24] R. J. Williams, "Simple Statistical Gradient-Following Algorithms for Connectionist Reinforcement Learning," *Machine learning*, vol. 8, no. 3-4, pp. 229–256, 1992.
- [25] C. J. C. H. Watkins and P. Dayan, "Q-learning," *Machine Learning*, vol. 8, no. 3, pp. 279–292, 1992. [Online]. Available: <https://doi.org/10.1007/BF00992698>
- [26] D. Ormonet and S. Sen, "Kernel-Based Reinforcement Learning," *Machine Learning*, vol. 49, no. 2, pp. 161–178, 2002. [Online]. Available: <https://doi.org/10.1023/A:1017928328829>
- [27] X. Xu, D. Hu, and X. Lu, "Kernel-Based Least Squares Policy Iteration for Reinforcement Learning," *IEEE Transactions on Neural Networks*, vol. 18, no. 4, pp. 973–992, 2007.
- [28] Y. Engel, S. Mannor, and R. Meir, "Reinforcement Learning with Gaussian Processes," in *Proceedings of the 22nd International Conference on Machine Learning*. ACM, 2005, pp. 201–208.
- [29] G. Taylor and R. Parr, "Kernelized Value Function Approximation for Reinforcement Learning," in *Proceedings of the 26th International Conference on Machine Learning*, ser. ICML '09. ACM, 2009, pp. 1017–1024, event-place: Montreal, Quebec, Canada. [Online]. Available: <http://doi.acm.org/10.1145/1553374.1553504>
- [30] O. B. Kroemer and J. R. Peters, "A Non-Parametric Approach to Dynamic Programming," in *Advances in Neural Information Processing Systems*. Curran Associates, Inc., 2011, pp. 1719–1727. [Online]. Available: <http://papers.nips.cc/paper/4182-a-non-parametric-approach-to-dynamic-programming.pdf>
- [31] F. Borrelli, A. Bemporad, and M. Morari, *Predictive Control for Linear and Hybrid Systems*. Cambridge University Press, Jun. 2017, google-Books-ID: 7NUoDwAAQBAJ.
- [32] E. A. Nadaraya, "On Estimating Regression," *Theory of Probability & Its Applications*, vol. 9, no. 1, pp. 141–142, 1964.
- [33] G. S. Watson, "Smooth Regression Analysis," *Sankhyā: The Indian Journal of Statistics, Series A*, pp. 359–372, 1964.
- [34] J. Fan, "Design-Adaptive Nonparametric Regression," *Journal of the American Statistical Association*, vol. 87, no. 420, pp. 998–1004, 1992.
- [35] L. Wasserman, *All of Nonparametric Statistics*. Springer, 2006. [Online]. Available: <https://books.google.it/books?hl=it&lr=&id=MRFlzQfRg7UC&oi=fnd&pg=PA2&dq=wasserman+2006+all&ots=SP5Qp53XJz&sig=R9JPan0NnS8GkezXCj85U2ndFmc#v=onepage&q=wasserman%202006%20all&f=false>
- [36] S. Tosatto, R. Akrou, and J. Peters, "An Upper Bound of the Bias of Nadaraya-Watson Kernel Regression under Lipschitz Assumptions," *arXiv preprint arXiv:2001.10972*, 2020.
- [37] J. Peters, K. Mulling, and Y. Altun, "Relative Entropy Policy Search," in *Twenty-Fourth AAAI Conference on Artificial Intelligence*, 2010.
- [38] J. Schulman, F. Wolski, P. Dhariwal, A. Radford, and O. Klimov, "Proximal Policy Optimization Algorithms," *arXiv preprint arXiv:1707.06347*, 2017.
- [39] A. M. Metelli, M. Papini, F. Faccio, and M. Restelli, "Policy Optimization via Importance Sampling," in *Advances in Neural Information Processing Systems*. Curran Associates, Inc., 2018, pp. 5442–5454. [Online]. Available: <http://papers.nips.cc/paper/7789-policy-optimization-via-importance-sampling.pdf>
- [40] K. Chua, R. Calandra, R. McAllister, and S. Levine, "Deep Reinforcement Learning in a Handful of Trials using Probabilistic Dynamics Models," in *Advances in Neural Information Processing Systems*. Curran Associates, Inc., 2018, pp. 4754–4765.
- [41] A. Antos, R. Munos, and C. Szepesvari, "Fitted Q-Iteration in Continuous Action-Space MDPs," in *Neural Information Processing Systems*, 2007.
- [42] O. Kroemer, E. Ugur, E. Oztop, and J. Peters, "A Kernel-Based Approach to Direct Action Perception," in *International Conference on Robotics and Automation*. IEEE, 2012, pp. 2605–2610.
- [43] J. Baxter and P. L. Bartlett, "Infinite-Horizon Policy-Gradient Estimation," *Journal of Artificial Intelligence Research*, vol. 15, pp. 319–350, 2001.
- [44] S. Kakade, "A Natural Policy Gradient," in *Proceedings of the 14th International Conference on Neural Information Processing Systems*, 2001, pp. 1531–1538.
- [45] J. Peters and S. Schaal, "Natural Actor-Critic," *Neurocomputing*, vol. 71, no. 7-9, pp. 1180–1190, 2008, publisher: Elsevier.
- [46] A. B. Owen, *Monte Carlo Theory, Methods and Examples*, 2013.
- [47] R. S. Sutton, A. R. Mahmood, and M. White, "An Emphatic Approach to the Problem of Off-Policy Temporal-Difference Learning," *The Journal of Machine Learning Research*, vol. 17, no. 1, pp. 2603–2631, 2016, publisher: JMLR.org.
- [48] Q. Liu, L. Li, Z. Tang, and D. Zhou, "Breaking the Curse of Horizon: Infinite-Horizon Off-Policy Estimation," in *Advances in Neural Information Processing Systems*, 2018, pp. 5356–5366.
- [49] Y. Liu, A. Swaminathan, A. Agarwal, and E. Brunskill, "Off-Policy Policy Gradient with State Distribution Correction," *arXiv:1904.08473*, 2019, arXiv: 1904.08473. [Online]. Available: <http://arxiv.org/abs/1904.08473>
- [50] O. Nachum, B. Dai, I. Kostrikov, Y. Chow, L. Li, and D. Schuurmans, "AlgaeDICE: Policy Gradient from Arbitrary Experience," *arXiv:1912.02074v1*, 2019.
- [51] A. Argenson and G. Dulac-Arnold, "Model-Based Offline Planning," in *Proceeding of the 9th International Conference on Learning Representations*, 2020.
- [52] K. Lowrey, A. Rajeswaran, S. Kakade, E. Todorov, and I. Mordatch, "Plan Online, Learn Offline: Efficient Learning and Exploration via Model-Based Control," *arXiv preprint arXiv:1811.01848*, 2018.
- [53] G. Brockman, V. Cheung, L. Pettersson, J. Schneider, J. Schulman, J. Tang, and W. Zaremba, "OpenAI Gym," *arXiv:1606.01540*, 2016, arXiv: 1606.01540. [Online]. Available: <http://arxiv.org/abs/1606.01540>
- [54] J. Fu, A. Kumar, O. Nachum, G. Tucker, and S. Levine, "D4rl: Datasets for Deep Data-Driven Reinforcement Learning," *arXiv preprint arXiv:2004.07219*, 2020.
- [55] E. Todorov, T. Erez, and Y. Tassa, "MuJoCo: A Physics Engine for Model-Based Control," in *2012 IEEE/RSJ International Conference on Intelligent Robots and Systems*. IEEE, 2012, pp. 5026–5033.
- [56] C. R. Shelton, "Policy Improvement for POMDPs Using Normalized Importance Sampling," *arXiv preprint arXiv:1301.2310*, 2013.
- [57] R. Y. Rubinstein and D. P. Kroese, *Simulation and the Monte Carlo Method*. John Wiley & Sons, 2016, vol. 10.
- [58] T. Jie and P. Abbeel, "On a Connection Between Importance Sampling and the Likelihood Ratio Policy Gradient," in *Advances in Neural Information Processing Systems*, 2010, pp. 1000–1008.
- [59] P. Thomas, "Bias in Natural Actor-Critic Algorithms," in *International Conference on Machine Learning*, 2014, pp. 441–448.

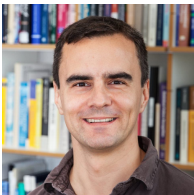
- [60] C. Nota and P. S. Thomas, "Is the Policy Gradient a Gradient?" in *Proceedings of the 19th International Conference on Autonomous Agents and Multiagent Systems*, 2020.
- [61] C. D'Eramo, D. Tateo, A. Bonarini, M. Restelli, and J. Peters, *MushroomRL: Simplifying Reinforcement Learning Research*, 2020, publication Title: arXiv preprint arXiv:2001.01102. [Online]. Available: <https://github.com/MushroomRL/mushroom-rl>
- [62] J. Kober and J. R. Peters, "Policy Search for Motor Primitives in Robotics," in *Advances in Neural Information Processing Systems*, 2009, pp. 849–856.



Samuele Tosatto received his Ph.D. in Computer Science from the Technical University of Darmstadt in 2020. He previously obtained his M.Sc. in the Polytechnic University of Milan. He is currently a post-doc fellow with the University of Alberta, working in the Reinforcement Learning and Artificial Intelligence group. His research interests center around reinforcement learning with a focus on its application to real robotic systems.



João Carvalho is currently a Ph.D. student at the Intelligent Autonomous Systems group of the Technical University of Darmstadt. Previously, he completed a M.Sc. degree in Computer Science from the Albert-Ludwigs-Universität Freiburg, and studied Electrical and Computer Engineering at the Instituto Superior Técnico of the University of Lisbon. His research is focused on learning algorithms for control and robotics.



Jan Peters is a full professor (W3) for Intelligent Autonomous Systems at the Computer Science Department of the Technical University of Darmstadt. He has been a senior research scientist and group leader at the MaxPlanck Institute for Intelligent Systems, where he headed the inter-departmental Robot Learning Group. Jan Peters has received the Dick Volz Best 2007 US Ph.D. Thesis Runner-Up Award, the Robotics: Science & Systems - Early Career Spotlight, the INNS Young Investigator Award, and the IEEE

Robotics & Automation Society's Early Career Award as well as numerous best paper awards. In 2015, he received an ERC Starting Grant and in 2019, he was appointed as an IEEE Fellow.

APPENDIX

1 SUPPORT TO THE THEORETICAL ANALYSIS

1.1 Existence and Uniqueness of the Fixed Point of the Nonparametric Bellman Equation

In the following, we discuss the existence and uniqueness of the solution of the nonparametric Bellman equation (NPBE). To do so, we will first notice that the solution must be a linear combination of the responsibility vector $\varepsilon_\pi(\mathbf{s})$, and therefore any solution of the NPBE must be bounded. We will also show that such a bound is $\pm R_{\max}/(1 - \gamma_c)$. We will use this bound to show that the solution must be unique. Subsequently, we will prove Theorem 1.

Proposition 1. Space of the Solution

The solution of the NPBE is $\varepsilon_\pi^\top(\mathbf{s})\mathbf{q}$ where $\mathbf{q} \in \mathbb{R}^n$, where n is the number of support points.

Informal Proof: The NPBE is

$$\hat{V}_\pi(\mathbf{s}) = \varepsilon_\pi^\top(\mathbf{s}) \left(\mathbf{r} + \int_{\mathcal{S}} \phi_\gamma(\mathbf{s}') \hat{V}_\pi(\mathbf{s}') ds' \right) \quad (12)$$

Both \mathbf{r} and $\int_{\mathcal{S}} \phi_\gamma(\mathbf{s}') \hat{V}_\pi(\mathbf{s}') ds'$ are constant w.r.t. \mathbf{s} , therefore $\hat{V}_\pi(\mathbf{s})$ must be a linear respect to $\varepsilon_\pi(\mathbf{s})$.

A first consequence of Proposition 1 is that, since $\varepsilon_\pi(\mathbf{s})$ is a vector of kernels, $\hat{V}_\pi(\mathbf{s})$ is bounded.

In Theorem 1 we state that the solution of the NPBE is $\hat{V}_\pi^*(\mathbf{s}) = \varepsilon_\pi^\top(\mathbf{s})\mathbf{\Lambda}_\pi^{-1}\mathbf{r}$. It is trivial to show that such a solution is a valid solution of the NPBE; however, the uniqueness of such a solution is non-trivial. In order to prove it, we will before show that if a solution to the NPBE exists, then the solution must be bounded by $[-R_{\max}/(1 - \gamma_c), R_{\max}/(1 - \gamma_c)]$, where $R_{\max} = \max_i |r_i|$. Note that this nice property is not common for other policy-evaluation algorithms (e.g., Neural Fitted Q -Iterations [5]).

Proposition 2. Bound of NPBE

If $V_\pi : \mathcal{S} \rightarrow \mathbb{R}$ is a solution to the NPBE, then $|V_\pi(\mathbf{s})| \leq R_{\max}/(1 - \gamma_c)$.

Proof. Suppose, by contradiction, that a function $f(\mathbf{s})$ is the solution of a NPBE, and that $\exists \mathbf{z} \in \mathcal{S} : f(\mathbf{z}) = R_{\max}/(1 - \gamma_c) + \epsilon$ where $\epsilon > 0$. Since the solution of the NPBE must be bounded, we can further assume without any loss of generality that $f(\mathbf{s}) \leq f(\mathbf{z})$. Then,

$$\frac{R_{\max}}{1 - \gamma_c} + \epsilon = \varepsilon_\pi^\top(\mathbf{z})\mathbf{r} + \varepsilon_\pi^\top(\mathbf{z}) \int_{\mathcal{S}} \phi_\gamma(\mathbf{s}') f(\mathbf{s}') ds'.$$

Since by assumption the previous equation must be fulfilled, and $\varepsilon_\pi(\mathbf{z})$ is a stochastic vector, $|\varepsilon_\pi^\top(\mathbf{z})\mathbf{r}| \leq R_{\max}$, we have

$$\left| \frac{R_{\max}}{1 - \gamma_c} + \epsilon - \varepsilon_\pi^\top(\mathbf{z}) \int_{\mathcal{S}} \phi_\gamma(\mathbf{s}') f(\mathbf{s}') ds' \right| \leq R_{\max}. \quad (13)$$

However, noticing also that $0 \leq \phi_i^{\pi, \gamma}(\mathbf{s}) \leq \gamma_c$, we have

$$\begin{aligned} \frac{R_{\max}}{1 - \gamma_c} + \epsilon - \varepsilon_\pi^\top(\mathbf{z}) \int_{\mathcal{S}} \phi_\gamma(\mathbf{s}') f(\mathbf{s}') ds' &\geq \frac{R_{\max}}{1 - \gamma_c} + \epsilon - \gamma_c \max_{\mathbf{s}} f(\mathbf{s}) \\ &\geq \frac{R_{\max}}{1 - \gamma_c} + \epsilon - \gamma_c \frac{R_{\max}}{1 - \gamma_c} \\ &= R_{\max} + \epsilon, \end{aligned}$$

which is in contradiction with Equation 13. A completely symmetric proof can be derived assuming by contradiction that $\exists \mathbf{z} \in \mathcal{S} : f(\mathbf{z}) = -R_{\max}/(1 - \gamma_c) - \epsilon$ and $f(\mathbf{s}) \geq f(\mathbf{z})$. \square

Proposition 3. If \mathbf{r} is bounded by R_{\max} and if $f^* : \mathcal{S} \rightarrow \mathbb{R}$ satisfies the NPBE, then there is no other function $f : \mathcal{S} \rightarrow \mathbb{R}$ for which $\exists \mathbf{z} \in \mathcal{S}$ and $|f^*(\mathbf{z}) - f(\mathbf{z})| > 0$.

Proof. Suppose, by contradiction, that exists a function $g : \mathcal{S} \rightarrow \mathbb{R}$ such that $f^*(\mathbf{s}) + g(\mathbf{s})$ satisfies Equation 12. Furthermore assume that $\exists \mathbf{z} : g(\mathbf{z}) \neq 0$. Note that, since $f : \mathcal{S} \rightarrow \mathbb{R}$ is a solution of the NPBE, then

$$\int_{\mathcal{S}} \varepsilon_\pi^\top(\mathbf{s}) \phi_\gamma(\mathbf{s}') f^*(\mathbf{s}') ds' \in \mathbb{R}, \quad (14)$$

and similarly

$$\int_{\mathcal{S}} \varepsilon_\pi^\top(\mathbf{s}) \phi_\gamma(\mathbf{s}') (f^*(\mathbf{s}') + g(\mathbf{s}')) ds' \in \mathbb{R}. \quad (15)$$

The existence of the integrals in Equations 14 and 15 implies

$$\int_{\mathcal{S}} \varepsilon_\pi^\top(\mathbf{s}) \phi_\gamma(\mathbf{s}') g(\mathbf{s}') ds' \in \mathbb{R}. \quad (16)$$

Note that

$$\begin{aligned}
|g(\mathbf{s})| &= |f^*(\mathbf{s}) - (f^*(\mathbf{s}) + g(\mathbf{s}))| \\
&= \left| f^*(\mathbf{s}) - \boldsymbol{\varepsilon}_\pi^\top(\mathbf{s}) \left(\mathbf{r} + \int_{\mathcal{S}} \phi_\gamma(\mathbf{s}') (f^*(\mathbf{s}') + g(\mathbf{s}')) \, \mathrm{d}\mathbf{s}' \right) \right| \\
&= \left| \boldsymbol{\varepsilon}_\pi^\top(\mathbf{s}) \left(\mathbf{r} + \int_{\mathcal{S}} \phi_\gamma(\mathbf{s}') f^*(\mathbf{s}') \, \mathrm{d}\mathbf{s}' \right) - \boldsymbol{\varepsilon}_\pi^\top(\mathbf{s}) \left(\mathbf{r} + \int_{\mathcal{S}} \phi_\gamma(\mathbf{s}') (f^*(\mathbf{s}') + g(\mathbf{s}')) \, \mathrm{d}\mathbf{s}' \right) \right| \\
&= \left| \boldsymbol{\varepsilon}_\pi^\top(\mathbf{s}) \int_{\mathcal{S}} \phi_\gamma(\mathbf{s}') g(\mathbf{s}') \, \mathrm{d}\mathbf{s}' \right| \\
&= \left| \boldsymbol{\varepsilon}_\pi^\top(\mathbf{s}) \int_{\mathcal{S}} \phi_\gamma(\mathbf{s}') g(\mathbf{s}') \, \mathrm{d}\mathbf{s}' \right|.
\end{aligned}$$

Using Jensen's inequality

$$|g(\mathbf{s})| \leq \boldsymbol{\varepsilon}_\pi^\top(\mathbf{s}) \int_{\mathcal{S}} \phi_\gamma(\mathbf{s}') |g(\mathbf{s}')| \, \mathrm{d}\mathbf{s}'.$$

Since both f^* and $f + g$ are bounded by $\frac{R_{\max}}{1-\gamma_c}$, then $|g(\mathbf{s})| \leq A = \frac{2R_{\max}}{1-\gamma_c}$, then

$$\begin{aligned}
|g(\mathbf{s})| &\leq \boldsymbol{\varepsilon}_\pi^\top(\mathbf{s}) \int_{\mathcal{S}} \phi_\gamma(\mathbf{s}') |g(\mathbf{s}')| \, \mathrm{d}\mathbf{s}' \\
&\leq A \boldsymbol{\varepsilon}_\pi^\top(\mathbf{s}) \int_{\mathcal{S}} \phi_\gamma(\mathbf{s}') \, \mathrm{d}\mathbf{s}' \\
&\leq \gamma_c A.
\end{aligned} \tag{17}$$

We can iterate this reasoning now posing $|g(\mathbf{s})| \leq \gamma_c A$, and eventually we notice that $|g(\mathbf{s})| \leq 0$, which is in contradiction with the assumption made. \square

Proof of Theorem 1

Proof. Saying that \hat{V}_π^* is a solution for Equation 12 is equivalent to say

$$\hat{V}_\pi^*(\mathbf{s}) - \boldsymbol{\varepsilon}_\pi^\top(\mathbf{s}) \left(\mathbf{r} + \gamma \int_{\mathcal{S}} \phi_\gamma(\mathbf{s}') \hat{V}_\pi^*(\mathbf{s}') \, \mathrm{d}\mathbf{s}' \right) = 0 \quad \forall \mathbf{s} \in \mathcal{S}.$$

We can verify that by simple algebraic manipulation

$$\begin{aligned}
&\hat{V}_\pi^*(\mathbf{s}) - \boldsymbol{\varepsilon}_\pi^\top(\mathbf{s}) \left(\mathbf{r} + \int_{\mathcal{S}} \phi_\gamma(\mathbf{s}') \hat{V}_\pi^*(\mathbf{s}') \, \mathrm{d}\mathbf{s}' \right) \\
&= \boldsymbol{\varepsilon}_\pi^\top(\mathbf{s}) \boldsymbol{\Lambda}_\pi^{-1} \mathbf{r} - \boldsymbol{\varepsilon}_\pi^\top(\mathbf{s}) \left(\mathbf{r} + \int_{\mathcal{S}} \phi_\gamma(\mathbf{s}') \boldsymbol{\varepsilon}_\pi^\top(\mathbf{s}') \boldsymbol{\Lambda}_\pi^{-1} \mathbf{r} \, \mathrm{d}\mathbf{s}' \right) \\
&= \boldsymbol{\varepsilon}_\pi^\top(\mathbf{s}) \left(\boldsymbol{\Lambda}_\pi^{-1} \mathbf{r} - \mathbf{r} - \int_{\mathcal{S}} \phi_\gamma(\mathbf{s}') \boldsymbol{\varepsilon}_\pi^\top(\mathbf{s}') \boldsymbol{\Lambda}_\pi^{-1} \mathbf{r} \, \mathrm{d}\mathbf{s}' \right) \\
&= \boldsymbol{\varepsilon}_\pi^\top(\mathbf{s}) \left(\left(I - \int_{\mathcal{S}} \phi_\gamma(\mathbf{s}') \boldsymbol{\varepsilon}_\pi^\top(\mathbf{s}') \, \mathrm{d}\mathbf{s}' \right) \boldsymbol{\Lambda}_\pi^{-1} \mathbf{r} - \mathbf{r} \right) \\
&= \boldsymbol{\varepsilon}_\pi^\top(\mathbf{s}) \left(\boldsymbol{\Lambda}_\pi \boldsymbol{\Lambda}_\pi^{-1} \mathbf{r} - \mathbf{r} \right) \\
&= 0.
\end{aligned} \tag{18}$$

Since equation 12 has (at least) one solution, Proposition 3 guarantees that the solution (\hat{V}_π^*) is unique. \square

1.2 Bias of the Nonparametric Bellman Equation

In this section, we want to show the findings of Theorem 3. To do so, we introduce the infinite-samples extension of the NPBE.

Proposition 4. *Let us suppose to have a dataset of infinite samples, and in particular one sample for each state-action pair of the state-action space. In the limit of infinite samples the NPBE defined in Definition 2 with a data-set $\lim_{n \rightarrow \infty} D_n$ collected under distribution β on the state-action space and MDP \mathcal{M} converges to*

$$\begin{aligned}
V_D(\mathbf{s}) &= \lim_{n \rightarrow \infty} \int_{\mathcal{A}} \frac{\sum_{i=1}^n \psi_i(\mathbf{s}) \varphi_i(\mathbf{a}) \left(r_i + \gamma_i \int_{\mathcal{S}} \phi_i(\mathbf{s}') \hat{V}_\pi(\mathbf{s}') \, d\mathbf{s}' \right)}{\sum_{j=1}^n \psi_j(\mathbf{s}) \varphi_j(\mathbf{a})} \pi(\mathbf{a}|\mathbf{s}) \, d\mathbf{a} \\
&= \int_{\mathcal{A}} \frac{\lim_{n \rightarrow \infty} \frac{1}{n} \sum_{i=1}^n \psi_i(\mathbf{s}) \varphi_i(\mathbf{a}) \left(r_i + \gamma_i \int_{\mathcal{S}} \phi_i(\mathbf{s}') \hat{V}_\pi(\mathbf{s}') \, d\mathbf{s}' \right)}{\lim_{n \rightarrow \infty} \frac{1}{n} \sum_{j=1}^n \psi_j(\mathbf{s}) \varphi_j(\mathbf{a})} \pi(\mathbf{a}|\mathbf{s}) \, d\mathbf{a} \\
&= \int_{\mathcal{A}} \frac{\int_{\mathcal{S} \times \mathcal{A}} \psi(\mathbf{s}, \mathbf{z}) \varphi(\mathbf{a}, \mathbf{b}) \left(R(\mathbf{z}, \mathbf{b}) + \int_{\mathcal{S}} \phi(\mathbf{s}', \mathbf{z}') p_\gamma(\mathbf{z}'|\mathbf{b}, \mathbf{z}) \hat{V}_\pi(\mathbf{s}') \, d\mathbf{s}' \right) \beta(\mathbf{z}, \mathbf{b}) \, d\mathbf{z} \, d\mathbf{b}}{\int_{\mathcal{S} \times \mathcal{A}} \psi(\mathbf{s}, \mathbf{z}) \varphi(\mathbf{a}, \mathbf{b}) \beta(\mathbf{z}, \mathbf{b}) \, d\mathbf{z} \, d\mathbf{b}} \pi(\mathbf{a}|\mathbf{s}) \, d\mathbf{a}. \quad (19)
\end{aligned}$$

If we impose the process generating samples to be non-degenerate distribution, and $-R_{\max} \leq R \leq R_{\max}$, we see that Propositions 1-3 remain valid. Furthermore, from Equation 19 we are able to infer that $\mathbb{E}_D[V_D(\mathbf{s})] = V_D(\mathbf{s})$ (since D is an infinite dataset, it does not matter if we re-sample it, the resulting value-function will be always the same).

Proof of Theorem 3. To keep the notation uncluttered, let us introduce

$$\varepsilon(\mathbf{s}, \mathbf{a}, \mathbf{z}, \mathbf{b}) = \frac{\psi(\mathbf{s}, \mathbf{z}) \varphi(\mathbf{a}, \mathbf{b}) \beta(\mathbf{z}, \mathbf{b})}{\int_{\mathcal{S} \times \mathcal{A}} \psi(\mathbf{s}, \mathbf{z}) \varphi(\mathbf{a}, \mathbf{b}) \beta(\mathbf{z}, \mathbf{b}) \, d\mathbf{z} \, d\mathbf{b}}. \quad (20)$$

We want to bound

$$\begin{aligned}
\bar{V}(\mathbf{s}) - V^*(\mathbf{s}) &= \int_{\mathcal{A}} \left(\int \varepsilon(\mathbf{s}, \mathbf{a}, \mathbf{z}, \mathbf{b}) R(\mathbf{z}, \mathbf{b}) \, d\mathbf{z} \, d\mathbf{b} + \int_{\mathcal{S} \times \mathcal{A}} \varepsilon(\mathbf{s}, \mathbf{a}, \mathbf{z}, \mathbf{b}) \int_{\mathcal{S}} \phi_i(\mathbf{s}', \mathbf{z}') p_\gamma(\mathbf{z}'|\mathbf{b}, \mathbf{z}) \bar{V}(\mathbf{s}') \, d\mathbf{s}' \, d\mathbf{z} \, d\mathbf{b} \right. \\
&\quad \left. - R(\mathbf{s}, \mathbf{a}) - \int_{\mathcal{S}} V^*(\mathbf{s}') p_\gamma(\mathbf{s}'|\mathbf{s}, \mathbf{a}) \, d\mathbf{s}' \right) \pi(\mathbf{a}|\mathbf{s}) \, d\mathbf{a}
\end{aligned}$$

$$\begin{aligned}
\Rightarrow |\bar{V}(\mathbf{s}) - V^*(\mathbf{s})| &\leq \max_{\mathbf{a}} \left| \int \varepsilon(\mathbf{s}, \mathbf{a}, \mathbf{z}, \mathbf{b}) (R(\mathbf{z}, \mathbf{b}) - R(\mathbf{s}, \mathbf{a})) \, d\mathbf{z} \, d\mathbf{b} \right| \\
&\quad + \max_{\mathbf{a}} \left| \int_{\mathcal{S}} p_\gamma(\mathbf{z}'|\mathbf{b}, \mathbf{z}) (\phi_i(\mathbf{s}', \mathbf{z}') \bar{V}(\mathbf{s}') - V^*(\mathbf{s}')) \, d\mathbf{z} \, d\mathbf{b} \right| \quad (21)
\end{aligned}$$

$$\leq \max_{\mathbf{a}} \underbrace{\left| \int \varepsilon(\mathbf{s}, \mathbf{a}, \mathbf{z}, \mathbf{b}) (R(\mathbf{z}, \mathbf{b}) - R(\mathbf{s}, \mathbf{a})) \, d\mathbf{z} \, d\mathbf{b} \right|}_A \quad (22)$$

$$\begin{aligned}
&\quad + \gamma_c \max_{\mathbf{a}} \underbrace{\left| \int_{\mathcal{S} \times \mathcal{A}} \varepsilon(\mathbf{s}, \mathbf{a}, \mathbf{z}, \mathbf{b}) \int_{\mathcal{S}} p(\mathbf{z}'|\mathbf{b}, \mathbf{z}) (\phi_i(\mathbf{s}', \mathbf{z}') \bar{V}(\mathbf{s}') - V^*(\mathbf{s}')) \, d\mathbf{s}' \, d\mathbf{z} \, d\mathbf{b} \right|}_B \\
&= \mathbf{A}_{\text{Bias}} + \gamma_c \mathbf{B}_{\text{Bias}} \quad (23)
\end{aligned}$$

Term A is the bias of Nadaraya-Watson kernel regression, as it is possible to observe in [36], therefore Theorem 2 applies

$$\mathbf{A}_{\text{Bias}} = \frac{L_R \sum_{k=1}^d \mathbf{h}_k \left(\prod_{i \neq k}^d e^{\frac{L_\beta^2 \mathbf{h}_i^2}{2}} \left(1 + \operatorname{erf} \left(\frac{\mathbf{h}_i L_\beta}{\sqrt{2}} \right) \right) \right) \left(\frac{1}{\sqrt{2\pi}} + L_\beta \mathbf{h}_k e^{\frac{L_\beta^2 \mathbf{h}_k^2}{2}} \left(1 + \operatorname{erf} \left(\frac{\mathbf{h}_k L_\beta}{\sqrt{2}} \right) \right) \right)}{\prod_{i=1}^d e^{\frac{L_\beta^2 \mathbf{h}_i^2}{2}} \left(1 - \operatorname{erf} \left(\frac{\mathbf{h}_i L_\beta}{\sqrt{2}} \right) \right)},$$

where $\mathbf{h} = [\mathbf{h}_\psi, \mathbf{h}_\varphi]$ and $d = d_s + d_a$.

$$\begin{aligned}
B_{\text{bias}} &\leq \gamma_c \max_{\mathbf{a}} \left| \frac{\int_{\mathcal{S} \times \mathcal{A}} \psi(\mathbf{s}, \mathbf{z}) \varphi(\mathbf{a}, \mathbf{b}) \left(\int_{\mathcal{S} \times \mathcal{S}} \bar{V}(\mathbf{z}') \phi(\mathbf{z}', \mathbf{s}') p(\mathbf{s}' | \mathbf{s}, \mathbf{a}) \, ds' \, dz' - \int_{\mathcal{S}} V^*(\mathbf{s}') p(\mathbf{s}' | \mathbf{s}, \mathbf{a}) \, ds' \right) \beta(\mathbf{z}, \mathbf{b}) \, dz \, db}{\int_{\mathcal{S}, \mathcal{A}} \psi(\mathbf{s}, \mathbf{z}) \varphi(\mathbf{a}, \mathbf{b}) \beta(\mathbf{z}, \mathbf{b}) \, dz \, db} \right| \\
&= \gamma_c \max_{\mathbf{a}} \left| \frac{\int_{\mathcal{S} \times \mathcal{A}} \psi(\mathbf{s}, \mathbf{z}) \varphi(\mathbf{a}, \mathbf{b}) \left(\int_{\mathcal{S}} \bar{V}(\mathbf{z}') \phi(\mathbf{z}', \mathbf{s}') - V^*(\mathbf{s}') \right) p(\mathbf{s}' | \mathbf{s}, \mathbf{a}) \, ds' \, dz' \right) \beta(\mathbf{z}, \mathbf{b}) \, dz \, db}{\int_{\mathcal{S}, \mathcal{A}} \psi(\mathbf{s}, \mathbf{z}) \varphi(\mathbf{a}, \mathbf{b}) \beta(\mathbf{z}, \mathbf{b}) \, dz \, db} \right| \\
&\leq \gamma_c \max_{\mathbf{a}, \mathbf{s}'} \left| \frac{\int_{\mathcal{S} \times \mathcal{A}} \psi(\mathbf{s}, \mathbf{z}) \varphi(\mathbf{a}, \mathbf{b}) \left(\int_{\mathcal{S}} \bar{V}(\mathbf{z}') \phi(\mathbf{z}', \mathbf{s}') - V^*(\mathbf{s}') \, dz' \right) \beta(\mathbf{z}, \mathbf{b}) \, dz \, db}{\int_{\mathcal{S}, \mathcal{A}} \psi(\mathbf{s}, \mathbf{z}) \varphi(\mathbf{a}, \mathbf{b}) \beta(\mathbf{z}, \mathbf{b}) \, dz \, db} \right| \\
&= \gamma_c \max_{\mathbf{a}, \mathbf{s}'} \left| \frac{\int_{\mathcal{S} \times \mathcal{A}} \psi(\mathbf{s}, \mathbf{z}) \varphi(\mathbf{a}, \mathbf{b}) \beta(\mathbf{z}, \mathbf{b}) \, dz \, db}{\int_{\mathcal{S}, \mathcal{A}} \psi(\mathbf{s}, \mathbf{z}) \varphi(\mathbf{a}, \mathbf{b}) \beta(\mathbf{z}, \mathbf{b}) \, dz \, db} \left(\int_{\mathcal{S}} \bar{V}(\mathbf{z}') \phi(\mathbf{z}', \mathbf{s}') - V^*(\mathbf{s}') \, dz' \right) \right| \\
&= \gamma_c \max_{\mathbf{s}'} \left| \int_{\mathcal{S}} \bar{V}(\mathbf{z}') \phi(\mathbf{z}', \mathbf{s}') - V^*(\mathbf{s}') \, dz' \right| \\
&= \gamma_c \max_{\mathbf{s}'} \left| \int_{\mathcal{S}} \bar{V}(\mathbf{s}' + \boldsymbol{\delta}) \phi(\mathbf{s}' + \boldsymbol{\delta}, \mathbf{s}') - V^*(\mathbf{s}') \, d\boldsymbol{\delta} \right|. \tag{24}
\end{aligned}$$

Note that

$$\phi(\mathbf{s}' + \boldsymbol{\delta}, \mathbf{s}') = \prod_{i=1}^{d_s} \frac{e^{-\frac{\delta_i^2}{2h_{\phi,i}^2}}}{\sqrt{2\pi h_{\phi,i}^2}},$$

thus, using the Lipschitz inequality,

$$\begin{aligned}
&\max_{\mathbf{s}'} \left| \int_{\mathcal{S}} \bar{V}(\mathbf{s}' + \boldsymbol{\delta}) \phi(\mathbf{s}' + \boldsymbol{\delta}, \mathbf{s}') - V^*(\mathbf{s}') \, d\boldsymbol{\delta} \right| \\
&\leq \max_{\mathbf{s}'} \left| \bar{V}(\mathbf{s}') - V^*(\mathbf{s}') \right| + \int_{\mathcal{S}} L_V \left(\sum_{i=1}^{d_s} |\delta_i| \right) \prod_{i=1}^{d_s} \frac{e^{-\frac{\delta_i^2}{2h_{\phi,i}^2}}}{\sqrt{2\pi h_{\phi,i}^2}} \, d\boldsymbol{\delta} \\
&= \max_{\mathbf{s}'} \left| \bar{V}(\mathbf{s}') - V^*(\mathbf{s}') \right| + L_V \int_{\mathcal{S}} \left(\sum_{i=1}^{d_s} |\delta_i| \right) \prod_{i=1}^{d_s} \frac{e^{-\frac{\delta_i^2}{2h_{\phi,i}^2}}}{\sqrt{2\pi h_{\phi,i}^2}} \, d\boldsymbol{\delta} \\
&= \max_{\mathbf{s}'} \left| \bar{V}(\mathbf{s}') - V^*(\mathbf{s}') \right| + L_V \sum_{k=1}^{d_s} \left(\prod_{i \neq k} \int_{-\infty}^{+\infty} \frac{e^{-\frac{\delta_i^2}{2h_{\phi,i}^2}}}{\sqrt{2\pi h_{\phi,i}^2}} \, d\delta_i \right) \int_{-\infty}^{+\infty} |\delta_k| \frac{e^{-\frac{\delta_k^2}{2h_{\phi,k}^2}}}{\sqrt{2\pi h_{\phi,k}^2}} \, d\delta_k \\
&= \max_{\mathbf{s}'} \left| \bar{V}(\mathbf{s}') - V^*(\mathbf{s}') \right| + L_V 2 \sum_{k=1}^{d_s} \int_0^{+\infty} \delta_k \frac{e^{-\frac{\delta_k^2}{2h_{\phi,k}^2}}}{\sqrt{2\pi h_{\phi,k}^2}} \, d\delta_k \\
&= \max_{\mathbf{s}'} \left| \bar{V}(\mathbf{s}') - V^*(\mathbf{s}') \right| + L_V \sum_{k=1}^{d_s} \frac{h_{\phi,k}}{\sqrt{2\pi}},
\end{aligned}$$

which means that

$$\left| \bar{V}(\mathbf{s}) - V^*(\mathbf{s}) \right| \leq A_{\text{Bias}} + \gamma_c \left(\max_{\mathbf{s}'} \left| \bar{V}(\mathbf{s}') - V^*(\mathbf{s}') \right| + L_V \sum_{k=1}^{d_s} \frac{h_{\phi,k}}{\sqrt{2\pi}} \right).$$

Since both $\bar{V}(\mathbf{s})$ and $V^*(\mathbf{s})$ are bounded by $-R_{\max}/(1-\gamma_c)$ and $R_{\max}(1-\gamma_c)$, then $|\bar{V}(\mathbf{s}) - V^*(\mathbf{s})| \leq 2\frac{R_{\max}}{1-\gamma_c}$, thus

$$\begin{aligned} |\bar{V}(\mathbf{s}) - V^*(\mathbf{s})| &\leq A_{\text{Bias}} + \gamma_c \left(\max_{\mathbf{s}'} |\bar{V}(\mathbf{s}') - V^*(\mathbf{s}')| + L_V \sum_{k=1}^{d_s} \frac{h_{\phi,k}}{\sqrt{2\pi}} \right) \\ |\bar{V}(\mathbf{s}) - V^*(\mathbf{s})| &\leq A_{\text{Bias}} + \gamma_c \left(2\frac{R_{\max}}{1-\gamma_c} + L_V \sum_{k=1}^{d_s} \frac{h_{\phi,k}}{\sqrt{2\pi}} \right) \\ \Rightarrow |\bar{V}(\mathbf{s}) - V^*(\mathbf{s})| &\leq A_{\text{Bias}} + \gamma_c \left(A_{\text{Bias}} + \gamma_c \left(2\frac{R_{\max}}{1-\gamma_c} + L_V \sum_{k=1}^{d_s} \frac{h_{\phi,k}}{\sqrt{2\pi}} \right) + L_V \sum_{k=1}^{d_s} \frac{h_{\phi,k}}{\sqrt{2\pi}} \right) \quad \text{using Equation (25)} \\ \Rightarrow |\bar{V}(\mathbf{s}) - V^*(\mathbf{s})| &\leq \sum_{t=0}^{\infty} \gamma_c^t \left(A_{\text{Bias}} + \gamma_c L_V \sum_{k=1}^{d_s} \frac{h_{\phi,k}}{\sqrt{2\pi}} \right) \quad \text{using Equation (25)} \\ \Rightarrow |\bar{V}(\mathbf{s}) - V^*(\mathbf{s})| &\leq \frac{1}{1-\gamma_c} \left(A_{\text{Bias}} + \gamma_c L_V \sum_{k=1}^{d_s} \frac{h_{\phi,k}}{\sqrt{2\pi}} \right). \end{aligned} \quad \square$$

2 SUPPORT TO THE EMPIRICAL ANALYSIS

2.1 Gradient Analysis

The parameters used for the LQG are

$$A = \begin{bmatrix} 1.2 & 0 \\ 0 & 1.1 \end{bmatrix}; \quad B = \begin{bmatrix} 1 & 0 \\ 0 & 1 \end{bmatrix}; \quad Q = \begin{bmatrix} 1 & 0 \\ 0 & 1 \end{bmatrix}; \quad R = \begin{bmatrix} 0.1 & 0 \\ 0 & 0.1 \end{bmatrix}; \quad \Sigma = \begin{bmatrix} 1 & 0 \\ 0 & 1 \end{bmatrix}; \quad \mathbf{s}_0 = [-1, -1].$$

The discount factor is $\gamma = 0.9$, and the length of the episodes is 50 steps. The parameters of the optimization policy are $\boldsymbol{\theta} = [-0.6, -0.8]$ and the off-policy parameters are $\boldsymbol{\theta}' = [-0.35, -0.5]$. The confidence intervals have been computed using *bootstrapped percentile intervals*. The size of the bootstrapped dataset vary from plot to plot (usually from 1000 to 5000 different seeds). The confidence intervals, instead, have been computed using 10000 bootstraps. We used this method instead the more classic standard error (using a χ^2 or a t -distribution), because often, due to the importance sampling, our samples are highly non-Gaussian and heavy-tailed. The bootstrapping method relies on less assumptions, and their confidence intervals were more precise in this case.

2.2 Policy Improvement analysis

We use a policy encoded as neural network with parameters $\boldsymbol{\theta}$. A deterministic policy is encoded with a neural network $\mathbf{a} = f_{\boldsymbol{\theta}}(\mathbf{s})$. The stochastic policy is encoded as a Gaussian distribution with parameters determined by a neural network with two outputs, the mean and covariance. In this case we represent by $f_{\boldsymbol{\theta}}(\mathbf{s})$ the slice of the output corresponding to the mean and by $g_{\boldsymbol{\theta}}(\mathbf{s})$ the part of the output corresponding to the covariance.

NOPG can be described with the following hyper-parameters

| NOPG Parameters | Meaning |
|----------------------------------|--|
| dataset sizes | number of samples contained in the dataset used for training |
| discount factor γ | discount factor in infinite horizon MDP |
| state \vec{h}_{factor} | constant used to decide the bandwidths for the state-space |
| action \vec{h}_{factor} | constant used to decide the bandwidths for the action-space |
| policy | parametrization of the policy |
| policy output | how is the output of the policy encoded |
| learning rate | the learning rate and the gradient ascent algorithm used |
| N_{π}^{MC} (NOPG-S) | number of samples drawn to compute the integral $\varepsilon_{\pi}(\mathbf{s})$ with MonteCarlo sampling |
| N_{ϕ}^{MC} | number of samples drawn to compute the integral over the next state $\int \phi(\mathbf{s}') d\mathbf{s}'$ |
| $N_{\mu_0}^{\text{MC}}$ | number of samples drawn to compute the integral over the initial distribution $\int \hat{V}_{\pi}(\mathbf{s}) \mu_0(\mathbf{s}) d\mathbf{s}$ |
| policy updates | number of policy updates before returning the optimized policy |

A few considerations about NOPG parameters. If $N_{\phi}^{\text{MC}} = 1$ we use the mean of the kernel ϕ as a sample to approximate the integral over the next state. When optimizing a stochastic policy represented by a Gaussian distribution, we set and linearly decay the variance over the policy optimization procedure. The kernel bandwidths are computed in two steps: first we find the best bandwidth for each dimension of the state and action spaces using cross validation; second we multiply

each bandwidth by an empirical constant factor (\vec{h}_{factor}). This second step is important to guarantee that the state and action spaces do not have a zero density. For instance, in a continuous action environment, when sampling actions from a uniform grid we have to guarantee that the space between the grid points have some density. The problem of estimating the bandwidth in kernel density estimation is well studied, but needs to be adapted to the problem at hand, specially with a low number of samples. We found this approach to work well for our experiments but it can be further improved.

2.2.1 Pendulum with Uniform Dataset

Tables 3 and 4 describe the hyper-parameters used to run the experiment shown in the first plot of Figure 9.

Dataset Generation: The datasets have been generated using a grid over the state-action spaces $\theta, \dot{\theta}, u$, where θ and $\dot{\theta}$ are respectively angle and angular velocity of the pendulum, and u is the torque applied. In Table 3 are enumerated the different datasets used.

| $\#\theta$ | $\#\dot{\theta}$ | $\#u$ | Sample size |
|------------|------------------|-------|-------------|
| 10 | 10 | 2 | 200 |
| 15 | 15 | 2 | 450 |
| 20 | 20 | 2 | 800 |
| 25 | 25 | 2 | 1250 |
| 30 | 30 | 2 | 1800 |
| 40 | 40 | 2 | 3200 |

TABLE 3: **Pendulum uniform grid dataset configurations** This table shows the level of discretization for each dimension of the state space ($\#\theta$ and $\#\dot{\theta}$) and the action space ($\#u$). Each line corresponds to a uniformly sampled dataset, where $\theta \in [-\pi, \pi]$, $\dot{\theta} \in [-8, 8]$ and $u \in [-2, 2]$. The entries under the states' dimensions and action dimension correspond to how many linearly spaced states or actions are to be queried from the corresponding intervals. The Cartesian product of states and actions dimensions is taken in order to generate the state-action pairs to query the environment transitions. The rightmost column indicates the total number of corresponding samples.

Algorithm details: The configuration used for NOPG-D and NOPG-S are listed in Table 4.

| NOPG | |
|----------------------------------|---|
| discount factor γ | 0.99 |
| state \vec{h}_{factor} | 1.0 1.0 1.0 |
| action \vec{h}_{factor} | 50.0 |
| policy | neural network parameterized by θ 1 hidden layer, 50 units, ReLU activations |
| policy output | 2 $\tanh(f_{\theta}(s))$ (NOGP-D) $\mu = 2 \tanh(f_{\theta}(s))$, $\sigma = \text{sigmoid}(g_{\theta}(s))$ (NOGP-S) |
| learning rate | 10^{-2} with ADAM optimizer |
| N_{π}^{MC} (NOPG-S) | 15 |
| N_{ϕ}^{MC} | 1 |
| $N_{\mu_0}^{\text{MC}}$ | (non applicable) fixed initial state |
| policy updates | $1.5 \cdot 10^3$ |

TABLE 4: **NOPG configurations for the Pendulum uniform grid experiment**

2.2.2 Pendulum with Random Agent

The following tables show the hyper-parameters used for generating the second plot starting from the left in Figure 9

| NOPG | |
|----------------------------------|---|
| dataset sizes | $10^2, 5 \cdot 10^2, 10^3, 1.5 \cdot 10^3, 2 \cdot 10^3, 3 \cdot 10^3, 5 \cdot 10^3, 7 \cdot 10^3, 9 \cdot 10^3, 10^4$ |
| discount factor γ | 0.99 |
| state \vec{h}_{factor} | 1.0 1.0 1.0 |
| action \vec{h}_{factor} | 25.0 |
| policy | neural network parameterized by θ 1 hidden layer, 50 units, ReLU activations |
| policy output | 2 $\tanh(f_{\theta}(s))$ (NOGP-D) $\mu = 2 \tanh(f_{\theta}(s))$, $\sigma = \text{sigmoid}(g_{\theta}(s))$ (NOGP-S) |
| learning rate | 10^{-2} with ADAM optimizer |

| | |
|----------------------------------|--------------------------------------|
| $N_{\pi_0}^{\text{MC}}$ (NOPG-S) | 10 |
| N_{ϕ}^{MC} | 1 |
| $N_{\mu_0}^{\text{MC}}$ | (non applicable) fixed initial state |
| policy updates | $2 \cdot 10^3$ |

SAC

| | |
|--------------------------|--|
| discount factor γ | 0.99 |
| rollout steps | 500 |
| actor | neural network parameterized by θ_{actor} 1 hidden layer, 50 units, ReLU activations |
| actor output | $2 \tanh(u)$, $u \sim \mathcal{N}(\cdot \mu = f_{\theta_{\text{actor}}}(\mathbf{s}), \sigma = g_{\theta_{\text{actor}}}(\mathbf{s}))$ |
| actor learning rate | 10^{-3} with ADAM optimizer |
| critic | neural network parameterized by θ_{critic} 2 hidden layers, 50 units, ReLU activations |
| critic output | $f_{\theta_{\text{critic}}}(\mathbf{s}, \mathbf{a})$ |
| critic learning rate | $5 \cdot 10^{-3}$ with ADAM optimizer |
| max replay size | $5 \cdot 10^5$ |
| initial replay size | 128 |
| batch size | 64 |
| soft update | $\tau = 5 \cdot 10^{-3}$ |
| policy updates | $2.5 \cdot 10^5$ |

DDPG / TD3

| | |
|--------------------------|---|
| discount factor γ | 0.99 |
| rollout steps | 500 |
| actor | neural network parameterized by θ_{actor} 1 hidden layer, 50 units, ReLU activations |
| actor output | $2 \tanh(f_{\theta_{\text{actor}}}(\mathbf{s}))$ |
| actor learning rate | 10^{-3} with ADAM optimizer |
| critic | neural network parameterized by θ_{critic} 2 hidden layers, 50 units, ReLU activations |
| critic output | $f_{\theta_{\text{critic}}}(\mathbf{s}, \mathbf{a})$ |
| critic learning rate | 10^{-2} with ADAM optimizer |
| max replay size | $5 \cdot 10^5$ |
| initial replay size | 128 |
| batch size | 64 |
| soft update | $\tau = 5 \cdot 10^{-3}$ |
| policy updates | $2.5 \cdot 10^5$ |

PWIS

| | |
|--------------------------|---|
| dataset sizes | $10^2, 5 \cdot 10^2, 10^3, 2 \cdot 10^3, 5 \cdot 10^3, 7.5 \cdot 10^3,$ $10^4, 1.2 \cdot 10^4, 1.5 \cdot 10^4, 2 \cdot 10^4, 2.5 \cdot 10^4$ |
| discount factor γ | 0.99 |
| policy | neural network parameterized by θ 1 hidden layer, 50 units, ReLU activations |
| policy output | $\mu = 2 \tanh(f_{\theta}(\mathbf{s})), \sigma = \text{sigmoid}(g_{\theta}(\mathbf{s}))$ |
| learning rate | 10^{-2} with ADAM optimizer |
| policy updates | $2 \cdot 10^3$ |

BEAR

| | |
|--------------------------|---|
| dataset sizes | $10^2, 2 \cdot 10^2, 5 \cdot 10^2, 10^3, 2 \cdot 10^3, 5 \cdot 10^3,$ $10^4, 2 \cdot 10^4, 5 \cdot 10^4, 10^5$ |
| discount factor γ | 0.99 |
| policy | neural network parameterized by θ 1 hidden layer, 50 units, ReLU activations |

| | |
|--------------------------|--|
| policy output | $\mu = 2 \tanh(f_{\theta}(s)), \sigma = \text{sigmoid}(g_{\theta}(s))$ |
| learning rate | 10^{-4} |
| policy updates | $1 \cdot 10^3$ |
| <hr/> | |
| BRAC-(dual) | |
| dataset sizes | $10^2, 2 \cdot 10^2, 5 \cdot 10^2, 10^3, 2 \cdot 10^3, 5 \cdot 10^3, 10^4, 2 \cdot 10^4, 5 \cdot 10^4, 10^5$ |
| discount factor γ | 0.99 |
| policy | neural network parameterized by θ 1 hidden layer, 50 units, ReLU activations |
| policy output | $\mu = 2 \tanh(f_{\theta}(s)), \sigma = \text{sigmoid}(g_{\theta}(s))$ |
| learning rate | 10^{-3} with Adam |
| policy updates | $5 \cdot 10^4$ |
| batch size | ≤ 256 |
| soft update | $\tau = 5 \cdot 10^{-3}$ |
| <hr/> | |
| MOPO | |
| dataset sizes | $10^2, 2 \cdot 10^2, 5 \cdot 10^2, 10^3, 2 \cdot 10^3, 5 \cdot 10^3, 10^4, 2 \cdot 10^4, 5 \cdot 10^4, 10^5$ |
| discount factor γ | 0.99 |
| policy | neural network parameterized by θ 1 hidden layer, 50 units, ReLU activations |
| policy output | $\mu = 2 \tanh(f_{\theta}(s)), \sigma = \text{sigmoid}(g_{\theta}(s))$ |
| learning rate | $3 \cdot 10^{-4}$ with Adam |
| number of epochs | $5 \cdot 10^2$ |
| batch size | 256 |
| soft update | $\tau = 5 \cdot 10^{-3}$ |
| BNN hidden dims | 64 |
| BNN max epochs | 100 |
| BNN ensemble size | 7 |
| <hr/> | |
| MOReL | |
| dataset sizes | $10^2, 2 \cdot 10^2, 5 \cdot 10^2, 10^3, 2 \cdot 10^3, 5 \cdot 10^3, 10^4, 2 \cdot 10^4, 5 \cdot 10^4, 10^5$ |
| discount factor γ | 0.99 |
| policy | neural network parameterized by θ 1 hidden layer, 50 units, ReLU activations |
| policy output | $\mu = 2 \tanh(f_{\theta}(s)), \sigma = \text{sigmoid}(g_{\theta}(s))$ |
| step size | 0.02 |
| number of iterations | $1 \cdot 10^3$ |
| dynamics hidden dims | (128, 128), ReLU activations |
| dynamics lr | 0.001 |
| dynamics batch-size | 256 |
| dynamics fit-epochs | 25 |
| dynamics num-models | 4 |
| <hr/> | |

TABLE 5: Algorithms configurations for the Pendulum random data experiment

2.2.3 Cart-pole with Random Agent

The following tables show the hyper-parameters used to generate the third plot in Figure 9.

| NOPG | |
|----------------------------------|--|
| dataset sizes | $10^2, 2.5 \cdot 10^2, 5 \cdot 10^2, 10^3, 1.5 \cdot 10^3, 2.5 \cdot 10^3, 3 \cdot 10^3, 5 \cdot 10^3, 6 \cdot 10^3, 8 \cdot 10^3, 10^4$ |
| discount factor γ | 0.99 |
| state \vec{h}_{factor} | 1.0 1.0 1.0 |
| action \vec{h}_{factor} | 20.0 |
| policy | neural network parameterized by θ 1 hidden layer, 50 units, ReLU activations |
| policy output | $5 \tanh(f_{\theta}(s))$ (NOGP-D) $\mu = 5 \tanh(f_{\theta}(s)), \sigma = \text{sigmoid}(g_{\theta}(s))$ (NOGP-S) |
| learning rate | 10^{-2} with ADAM optimizer |
| N_{π}^{MC} (NOGP-S) | 10 |
| N_{ϕ}^{MC} | 1 |
| $N_{\mu_0}^{\text{MC}}$ | 15 |
| policy updates | $2 \cdot 10^3$ |

| SAC | |
|--------------------------|---|
| discount factor γ | 0.99 |
| rollout steps | 10000 |
| actor | neural network parameterized by θ_{actor} 1 hidden layer, 50 units, ReLU activations |
| actor output | $5 \tanh(u), u \sim \mathcal{N}(\cdot \mu = f_{\theta_{\text{actor}}}(s), \sigma = g_{\theta_{\text{actor}}}(s))$ |
| actor learning rate | 10^{-3} with ADAM optimizer |
| critic | neural network parameterized by θ_{critic} 2 hidden layers, 50 units, ReLU activations |
| critic output | $f_{\theta_{\text{critic}}}(s, \mathbf{a})$ |
| critic learning rate | $5 \cdot 10^{-3}$ with ADAM optimizer |
| max replay size | $5 \cdot 10^5$ |
| initial replay size | 128 |
| batch size | 64 |
| soft update | $\tau = 5 \cdot 10^{-3}$ |
| policy updates | $2.5 \cdot 10^5$ |

| DDPG / TD3 | |
|--------------------------|--|
| discount factor γ | 0.99 |
| rollout steps | 10000 |
| actor | neural network parameterized by θ_{actor} 1 hidden layer, 50 units, ReLU activations |
| actor output | $5 \tanh(f_{\theta_{\text{actor}}}(s))$ |
| actor learning rate | 10^{-3} with ADAM optimizer |
| critic | neural network parameterized by θ_{critic} 1 hidden layer, 50 units, ReLU activations |
| critic output | $f_{\theta_{\text{critic}}}(s, \mathbf{a})$ |
| critic learning rate | 10^{-2} with ADAM optimizer |
| soft update | $\tau = 10^{-3}$ |
| policy updates | $2 \cdot 10^5$ |

| PWIS | |
|--------------------------|--|
| dataset sizes | $10^2, 5 \cdot 10^2, 10^3, 2 \cdot 10^3, 3.5 \cdot 10^3, 5 \cdot 10^3, 8 \cdot 10^3, 10^4, 1.5 \cdot 10^4, 2 \cdot 10^4, 2.5 \cdot 10^4$ |
| discount factor γ | 0.99 |
| policy | neural network parameterized by θ 1 hidden layer, 50 units, ReLU activations |
| policy output | $\mu = 5 \tanh(f_{\theta}(s)), \sigma = \text{sigmoid}(g_{\theta}(s))$ |
| learning rate | 10^{-3} with ADAM optimizer |

| | |
|----------------|----------------|
| policy updates | $2 \cdot 10^3$ |
|----------------|----------------|

| BEAR | |
|--------------------------|--|
| dataset sizes | $10^2, 2 \cdot 10^2, 5 \cdot 10^2, 10^3, 2 \cdot 10^3, 5 \cdot 10^3, 10^4, 2 \cdot 10^4, 5 \cdot 10^4, 10^5$ |
| discount factor γ | 0.99 |
| policy | neural network parameterized by θ 1 hidden layer, 50 units, ReLU activations |
| policy output | $\mu = 5 \tanh(f_\theta(\mathbf{s})), \sigma = \text{sigmoid}(g_\theta(\mathbf{s}))$ |
| learning rate | 10^{-4} |
| policy updates | $1 \cdot 10^3$ |

| BRAC-(dual) | |
|--------------------------|--|
| dataset sizes | $10^2, 2 \cdot 10^2, 5 \cdot 10^2, 10^3, 2 \cdot 10^3, 5 \cdot 10^3, 10^4, 2 \cdot 10^4, 5 \cdot 10^4, 10^5$ |
| discount factor γ | 0.99 |
| policy | neural network parameterized by θ 1 hidden layer, 50 units, ReLU activations |
| policy output | $\mu = 5 \tanh(f_\theta(\mathbf{s})), \sigma = \text{sigmoid}(g_\theta(\mathbf{s}))$ |
| learning rate | 10^{-3} with Adam |
| policy updates | $5 \cdot 10^4$ |
| batch size | ≤ 256 |
| soft update | $\tau = 5 \cdot 10^{-3}$ |

| MOPO | |
|--------------------------|--|
| dataset sizes | $10^2, 2 \cdot 10^2, 5 \cdot 10^2, 10^3, 2 \cdot 10^3, 5 \cdot 10^3, 10^4, 2 \cdot 10^4, 5 \cdot 10^4, 10^5$ |
| discount factor γ | 0.99 |
| policy | neural network parameterized by θ 1 hidden layer, 50 units, ReLU activations |
| policy output | $\mu = 2 \tanh(f_\theta(\mathbf{s})), \sigma = \text{sigmoid}(g_\theta(\mathbf{s}))$ |
| learning rate | $3 \cdot 10^{-4}$ with Adam |
| number of epochs | $5 \cdot 10^2$ |
| batch size | 256 |
| soft update | $\tau = 5 \cdot 10^{-3}$ |
| BNN hidden dims | 32 |
| BNN max epochs | 100 |
| BNN ensemble size | 7 |

| MOReL | |
|--------------------------|--|
| dataset sizes | $10^2, 2 \cdot 10^2, 5 \cdot 10^2, 10^3, 2 \cdot 10^3, 5 \cdot 10^3, 10^4, 2 \cdot 10^4, 5 \cdot 10^4, 10^5$ |
| discount factor γ | 0.99 |
| policy | neural network parameterized by θ 1 hidden layer, 50 units, ReLU activations |
| policy output | $\mu = 2 \tanh(f_\theta(\mathbf{s})), \sigma = \text{sigmoid}(g_\theta(\mathbf{s}))$ |
| step size | 0.02 |
| number of iterations | 500 |
| dynamics hidden dims | (128, 128), ReLU activations |
| dynamics lr | 0.001 |
| dynamics batch-size | 256 |
| dynamics fit-epochs | 25 |

dynamics num-models 4

TABLE 6: Algorithms configurations for the CartPole random data experiment.

2.2.4 U-Maze with D4RL

| NOPG | |
|----------------------------------|--|
| dataset sizes | $10^2, 3.5 \cdot 10^2, 5 \cdot 10^2, 6.5 \cdot 10^2, 8 \cdot 10^2, 1 \cdot 10^3$ |
| discount factor γ | 0.99 |
| state \vec{h}_{factor} | 2.0 |
| action \vec{h}_{factor} | 5.0 |
| policy | neural network parameterized by θ 2 hidden layers, 64 and 32 units, ReLU activations |
| policy output | $5 \tanh(f_{\theta}(s))$ (NOGP-D) $\mu = 5 \tanh(f_{\theta}(s)), \sigma = \text{sigmoid}(g_{\theta}(s))$ (NOGP-S) |
| learning rate | $3 \cdot 10^{-4}$ with ADAM optimizer |
| N_{π}^{MC} (NOGP-S) | 1 |
| N_{ϕ}^{MC} | 1 |
| $N_{\mu_0}^{\text{MC}}$ | 50 |
| policy updates | $5 \cdot 10^3$ |
| BEAR | |
| dataset sizes | $10^2, 2 \cdot 10^2, 5 \cdot 10^2, 10^3, 2 \cdot 10^3, 5 \cdot 10^3,$ $10^4, 2 \cdot 10^4, 5 \cdot 10^4, 10^5$ |
| discount factor γ | 0.99 |
| policy | neural network parameterized by θ 2 hidden layer, 64 and 32 units, ReLU activations |
| policy output | $\mu = 5 \tanh(f_{\theta}(s)), \sigma = \text{sigmoid}(g_{\theta}(s))$ |
| learning rate | 10^{-4} |
| policy updates | 10^3 |
| BRAC-(dual) | |
| dataset sizes | $10^2, 2 \cdot 10^2, 5 \cdot 10^2, 10^3, 2 \cdot 10^3, 5 \cdot 10^3,$ $10^4, 2 \cdot 10^4, 5 \cdot 10^4, 10^5$ |
| discount factor γ | 0.99 |
| policy | neural network parameterized by θ 2 hidden layer, 64 and 32 units, ReLU activations |
| policy output | $\mu = 5 \tanh(f_{\theta}(s)), \sigma = \text{sigmoid}(g_{\theta}(s))$ |
| learning rate | 10^{-3} with Adam |
| policy updates | $5 \cdot 10^4$ |
| batch size | ≤ 256 |
| soft update | $\tau = 5 \cdot 10^{-3}$ |
| MOPO | |
| dataset sizes | $10^2, 2 \cdot 10^2, 5 \cdot 10^2, 10^3, 2 \cdot 10^3, 5 \cdot 10^3,$ $10^4, 2 \cdot 10^4, 5 \cdot 10^4, 10^5$ |
| discount factor γ | 0.99 |
| policy | neural network parameterized by θ 2 hidden layer, 64 and 32 units, ReLU activations |
| policy output | $\mu = 5 \tanh(f_{\theta}(s)), \sigma = \text{sigmoid}(g_{\theta}(s))$ |
| learning rate | $3 \cdot 10^{-4}$ with Adam |
| number of epochs | $5 \cdot 10^2$ |
| batch size | 256 |
| soft update | $\tau = 5 \cdot 10^{-3}$ |
| BNN hidden dims | 64 |

| | |
|--------------------------|--|
| BNN max epochs | 100 |
| BNN ensemble size | 7 |
| <hr/> | |
| MOReL | |
| dataset sizes | $10^2, 2 \cdot 10^2, 5 \cdot 10^2, 10^3, 2 \cdot 10^3, 5 \cdot 10^3, 10^4, 2 \cdot 10^4, 5 \cdot 10^4, 10^5$ |
| discount factor γ | 0.99 |
| policy | neural network parameterized by θ (64, 32), ReLU activations |
| policy output | $\mu = 5 \tanh(f_\theta(\mathbf{s})), \sigma = \text{sigmoid}(g_\theta(\mathbf{s}))$ |
| step size | 0.005 |
| number of iterations | 500 |
| dynamics hidden dims | (32, 32), ReLU activations |
| dynamics lr | 0.001 |
| dynamics batch-size | 256 |
| dynamics fit-epochs | 25 |
| dynamics num-models | 4 |

TABLE 7: Algorithms configurations for the CartPole random data experiment.

2.2.5 Hopper with D4RL

| | |
|----------------------------------|---|
| NOPG | |
| dataset | hopper-expert-v2 |
| dataset sizes | $3 \cdot 10^3, 5 \cdot 10^3, 1 \cdot 10^4$ |
| discount factor γ | 0.99 |
| state \vec{h}_{factor} | 4.0 |
| action \vec{h}_{factor} | 10.0 |
| policy | neural network parameterized by θ 2 hidden layers, 256 and 256 units, ReLU activations |
| policy output | $\tanh(f_\theta(\mathbf{s}))$ (NOGP-D) $\mu = \tanh(f_\theta(\mathbf{s})), \sigma = \text{sigmoid}(g_\theta(\mathbf{s}))$ (NOGP-S) |
| learning rate | $3 \cdot 10^{-4}$ with ADAM optimizer |
| N_π^{MC} (NOGP-S) | 1 |
| N_ϕ^{MC} | 1 |
| $N_{\mu_0}^{\text{MC}}$ | 500 |
| policy updates | $5 \cdot 10^3$ |

2.2.6 Mountain Car with Human Demonstrator

The dataset (10 trajectories) for the experiment in Figure 11 has been generated by a human demonstrator, and is available in the source code provided.

| | |
|----------------------------------|---|
| NOPG | |
| discount factor γ | 0.99 |
| state \vec{h}_{factor} | 1.0 1.0 |
| action \vec{h}_{factor} | 50.0 |
| policy | neural network parameterized by $\vec{\theta}$ 1 hidden layer, 50 units, ReLU activations |
| policy output | $\tanh(f_{\vec{\theta}}(\mathbf{s}))$ (NOGP-D) $\mu = \tanh(f_{\vec{\theta}}(\mathbf{s})), \sigma = \text{sigmoid}(g_{\vec{\theta}}(\mathbf{s}))$ (NOGP-S) |
| learning rate | 10^{-2} with ADAM optimizer |

| | |
|--------------------------------|------------------|
| N_{π}^{MC} (NOPG-S) | 15 |
| N_{ϕ}^{MC} | 1 |
| $N_{\mu_0}^{\text{MC}}$ | 15 |
| policy updates | $1.5 \cdot 10^3$ |

TABLE 9: NOPG configurations for the MountainCar experiment.

2.3 Computational and Memory Complexity

Here we detail the computational and memory complexity of NOPG. We denote $N_{\mu_0}^{\text{MC}}$ Monte-Carlo samples for expectations under the initial state distribution, N_{π}^{MC} samples for expectations under the stochastic policy (for deterministic it is 1), and N_{ϕ}^{MC} samples for the expectations of each entry of $\hat{\mathbf{P}}_{\pi}^{\gamma}$. We keep the main constants throughout the analysis and drop constant factors, e.g. for the normalization of a matrix row, which involves summing up and diving each element of the row.

- Constructing the vector $\varepsilon_{\pi,0}$ takes $\mathcal{O}(N_{\mu_0}^{\text{MC}} N_{\pi}^{\text{MC}} n)$ time. Storing $\varepsilon_{\pi,0}$ occupies $\mathcal{O}(N_{\mu_0}^{\text{MC}} N_{\pi}^{\text{MC}} n)$ memory.
- We compute $\hat{\mathbf{P}}_{\pi}^{\gamma}$ row by row by sparsifying each row selecting the largest k elements, amounting to a complexity of $\mathcal{O}(N_{\phi}^{\text{MC}} N_{\pi}^{\text{MC}} n^2 \log k)$, with $k \ll n$, since the cost of processing one row is $\mathcal{O}(N_{\phi}^{\text{MC}} N_{\pi}^{\text{MC}} n \log k)$, e.g. with a Max-Heap, and there are n rows. Storing $\hat{\mathbf{P}}_{\pi}^{\gamma}$ needs $\mathcal{O}(N_{\phi}^{\text{MC}} N_{\pi}^{\text{MC}} n k)$ memory.
- We solve the linear system of equations $\mathbf{r} = \mathbf{\Lambda}_{\pi} \mathbf{q}_{\pi}$ and $\varepsilon_{\pi,0} = \mathbf{\Lambda}_{\pi}^{\top} \boldsymbol{\mu}_{\pi}$ for \mathbf{q}_{π} and $\boldsymbol{\mu}_{\pi}$ using the conjugate gradient method. Both computations take $\mathcal{O}(\sqrt{\delta}(k+1)n)$, where δ is the condition number of $\mathbf{\Lambda}_{\pi}$ after sparsification, and $(k+1)n$ the number of nonzero elements. The *plus one* comes from the computation of $\mathbf{\Lambda}_{\pi}$, since subtracting $\hat{\mathbf{P}}_{\pi}^{\gamma}$ from the identity matrix leads to an increase of n nonzero elements. The conjugate gradient method is specially advantageous when using sparse matrices. As a side note, computing the condition number δ is computationally intensive, but there exist methods to compute an upper bound.
- In computing the surrogate loss for the gradient computation, the cost of the vector-vector multiplication $\frac{\partial}{\partial \theta} \varepsilon_{\pi,0}^{\top} \mathbf{q}_{\pi}$ is $\mathcal{O}(N_{\mu_0}^{\text{MC}} N_{\pi}^{\text{MC}} n)$, and the vector-(sparse) matrix-vector multiplication $\boldsymbol{\mu}_{\pi}^{\top} \left(\frac{\partial}{\partial \theta} \hat{\mathbf{P}}_{\pi}^{\gamma} \right) \mathbf{q}_{\pi}$ is $\mathcal{O}(N_{\phi}^{\text{MC}} N_{\pi}^{\text{MC}} n^2 k)$, thus totaling $\mathcal{O}(N_{\mu_0}^{\text{MC}} N_{\pi}^{\text{MC}} n + N_{\phi}^{\text{MC}} N_{\pi}^{\text{MC}} n^2 k)$. Assuming the number of policy parameters M to be much lower than the number of samples, $M \ll n$, we ignore the gradient computation, since even when using finite differences, we would have $\mathcal{O}(M) \ll \mathcal{O}(n)$.

Even though the Monte-Carlo sample terms are fixed constants, and usually set to 1, we left these terms to emphasize that the policy parameters are inside each entry of $\varepsilon_{\pi,0}$ and $\hat{\mathbf{P}}_{\pi}^{\gamma}$, and thus we need to keep these terms until we compute the gradient with automatic differentiation. Since modern frameworks for gradient computation, such as Tensorflow or PyTorch, build a (static or dynamic) computational graph to backpropagate gradients, we cannot simply ignore these constants in terms of time and memory complexity. The only exception is when computing \mathbf{q}_{π} and $\boldsymbol{\mu}_{\pi}$ with the conjugate gradient. Since we do not need to backpropagate through this matrix, here we drop the Monte-Carlo terms because $\mathbf{\Lambda}_{\pi}$ is evaluated at the current policy parameters, leading to a matrix represented by $n \times k$ elements.

Taking all costs into account, we conclude that the computational complexity of NOPG *per policy update* is

$$\begin{aligned}
& \underbrace{\mathcal{O}(N_{\mu_0}^{\text{MC}} N_{\pi}^{\text{MC}} n)}_{\varepsilon_{\pi,0}} + \underbrace{\mathcal{O}(N_{\phi}^{\text{MC}} N_{\pi}^{\text{MC}} n^2 \log k)}_{\hat{\mathbf{P}}_{\pi}^{\gamma}} + \underbrace{\mathcal{O}(\sqrt{\delta}(k+1)n)}_{\text{conj. grad } \mathbf{q}_{\pi}, \boldsymbol{\mu}_{\pi}} \\
& + \underbrace{\mathcal{O}(N_{\mu_0}^{\text{MC}} N_{\pi}^{\text{MC}} n)}_{\frac{\partial}{\partial \theta} \varepsilon_{\pi,0}^{\top} \mathbf{q}_{\pi}} + \underbrace{\mathcal{O}(N_{\phi}^{\text{MC}} N_{\pi}^{\text{MC}} n^2 k)}_{\boldsymbol{\mu}_{\pi}^{\top} \frac{\partial}{\partial \theta} \hat{\mathbf{P}}_{\pi}^{\gamma} \mathbf{q}_{\pi}} \\
& = \mathcal{O}(N_{\mu_0}^{\text{MC}} N_{\pi}^{\text{MC}} n) + \mathcal{O}(N_{\phi}^{\text{MC}} N_{\pi}^{\text{MC}} n^2 (k + \log k)) + \mathcal{O}(\sqrt{\delta}(k+1)n).
\end{aligned}$$

The memory complexity is

$$\mathcal{O}(N_{\mu_0}^{\text{MC}} N_{\pi}^{\text{MC}} n) + \mathcal{O}(N_{\phi}^{\text{MC}} N_{\pi}^{\text{MC}} n k) + \underbrace{\mathcal{O}(n)}_{\mathbf{q}_{\pi}} + \underbrace{\mathcal{O}(n)}_{\boldsymbol{\mu}_{\pi}}.$$

The quantities in “underbrace” indicate the source of the complexities as described in the previous paragraphs. Hence, after dropping task-specific constants, the algorithm to implement NOPG has close to quadratic computational complexity and linear memory complexity with respect to the number of samples n , per policy update.